UNMANNED AERIAL SYSTEMS GUIDANCE AND CONTROL UTILIZING INSTANTANEOUS SCREW MOTION INVARIANTS

A THESIS SUBMITTED TO THE GRADUATE DIVISION OF THE UNIVERSITY OF HAWAIʻI AT MĀNOA IN PARTIAL FULFILLMENT OF THE REQUIREMENTS FOR THE DEGREE OF

MASTER OF SCIENCE

IN

MECHANICAL ENGINEERING

DECEMBER 2021

By

Jasur Abdinabiev

Thesis Committee:

Dilmurat Azimov, Chairperson
John Allen
Marcelo Kobayashi
Corey Ippolito

Keywords: instantaneous screw axis, quadcopter, invariants, UAV control

ACKNOWLEDGMENTS

I would like to acknowledge and thank Dr. Dilmurat Azimov for his valuable guidance, dedication, and endless support on the completion of this thesis. I am very grateful and fortunate to have been working with Dr. Azimov and gaining knowledge, skills, and professional experience from him.
I would also like to thank committee members for serving on my committee and giving thoughtful and helpful feedback, comments and suggestions.
I am grateful to all my friends and colleagues, Evan Kawamura, Minji Jo for their help and guidance.
I am grateful to Melissa Onishi for her instructions on mentorship and invitation to NHSEMP where I received a valuable mentoring experience.

ABSTRACT

The purpose of this research work is to study the applications of the instantaneous screw motion (ISM) concept to unmanned aerial system (UAS) dynamics, control, and guidance problems. Due to the potential use of this particular concept in dynamics and control problems, it is considered an essential subject to study. The advantages of this concept are that the ISM invariants are independent of the coordinate systems, and they can be expressed in terms of control parameters which allows us to find the control input and guidance commands without solving the traditional control problem. This research focuses on creating a framework for applications of the ISM concept in flight dynamics, control, and guidance problems in unmanned aerial vehicles (UAVs) by establishing the relationships between the ISM invariants and the dynamic and control parameters. A quadcopter and fixed-wing UAV models have been considered as an example of UAS. The expressions for the invariants have been derived using previous works. The motion of the instantaneous screw axis (ISA) has been studied, and the equations of motion have been derived. The method of defining the motion equations of the rigid body and the ISA as the functions of control parameters has been shown. The transition from the invariants to the traditional parameters (translational and rotational state parameters) has been represented. The profiles of the invariants and ISA have been obtained for several maneuvers of the quadcopter. The PD controller was utilized to simulate the results. The invariant description of a fixed-wing UAV motion on a vertical plane has been studied and the expressions for the invariants have been derived. Using the integrals obtained for this particular motion of a fixed-wing UAV, the invariants are found as the functions of the flight-path angle. An implicit relationship between the invariants and the parameters of flight dynamics (including the control parameters) has been established. The obtained results and expressions for the ISM invariants, flight dynamics, and control parameters can be used in control, guidance, and navigation problems.

CONTENTS

Acknowledgments . . . . . **ii**

Abstract . . . . . **iii**

List of Tables . . . . . **vi**

List of Figures . . . . . **vii**

1 Introduction **1**

1.1 Problem Statement 1

1.2 Literature Review 2

1.3 Overview of Chapters and Appendices 4

2 Unmanned Aerial Systems **5**

2.1 Quadcopter Dynamic Model 5

2.1.1 Kinematics 5

2.1.2 Forces and Torques 6

2.1.3 Equations of Motion 8

2.2 Fixed-wing UAV Dynamic Model 9

2.2.1 Equations of Motion 9

2.2.2 Control Parameters 11

3 Instantaneous Screw Motion Invariants **13**

3.1 Description of Invariants 13

3.2 Derivation of Invariants 13

3.3 Special Cases 18

3.3.1 Pure Translation 18

3.3.2 Pure Rotation 19

3.3.3 ISA with constant orientation: $\dot{\boldsymbol{\omega}} = \mathbf{0}$ 19

3.4 Inverse Problem 19

3.5 Motion of Instantaneous Screw Axis 20

4 ISM Invariants in Quadcopter Motion . . . 23
4.1 Control Problem in Quadcopter . . . 23
4.2 PD controller . . . 23
4.3 Other Controllers in Invariant Calculations . . . 24
4.4 Alternative Control Laws . . . 25
4.5 Profiles of ISM Parameters . . . 26
4.5.1 Example A: Transfer of Quadcopter . . . 26
4.5.2 Example B: Trajectory Follow . . . 34
5 ISM Invariants in Fixed-wing UAV Motion . . . 37
5.1 Expressions of Invariants . . . 37
5.2 Special Cases . . . 39
5.2.1 Rotational Motion . . . 39
5.2.2 Translational Motion . . . 40
5.3 Simulation . . . 40
5.3.1 Simulation Setup . . . 40
5.3.2 Graphical Relationship Between Parameters . . . 40
5.3.3 Discussions of Simulation Results . . . 41
5.4 Applications of the Study . . . 41
6 Guidance via ISM invariants . . . 46
7 Conclusions . . . 48
7.1 Conclusions of the Study . . . 48
7.2 Future works . . . 48
A Expression for v_3 . . . 49
B Expressions for i_4 and i_6 . . . 50
C Publications and Seminars . . . 51
C.1 Journal papers . . . 51
C.2 Seminars . . . 51
Bibliography . . . 52

LIST OF TABLES

4.1 Parameter values 25

4.2 Parameters for the PD controller. 25

C.1 List of Journal Papers 51

LIST OF FIGURES

1.1 Conventional GNC Loop and ISM-based Approach 1
1.2 Proposed GNC system with ISM invariants 2

2.1 Inertial and Body frames 5
2.2 Reynolds number for Small UAVs [1] 7

3.1 ISA in three consecutive time instants [2] 14
3.2 Screw parameters 15
3.3 Illustrations of Invariants for an instant of time 18
3.4 ISA in Cartesian coordinate system 20

4.1 Quadcopter Control Algorithm 24
4.2 State vector components 27
4.3 Profiles of Invariants 29
4.4 Profile of ISA 30
4.5 State vector 31
4.6 Profiles of Invariants 32
4.7 Profiles of the ISA 33
4.8 Network of tubes 34
4.9 Simulation results 35
4.10 Invariants 36

5.1 Invariants vs Angle of attack and Flight path angle 43
5.2 Control parameters and velocity 44
5.3 Invariants vs bank angle 45

6.1 Gravitational acceleration vs Altitude 47

6.2 Proposed GNC algorithm with ISM invariants 47

CHAPTER 1
INTRODUCTION

1.1 Problem Statement

Dynamic modeling, simplifications in the procedure, assumptions behind the simplifications, and kinematics are important factors in controlling a dynamical system. One group of complicated dynamical systems is unmanned aerial vehicles (UAV). When considering guidance, navigation, and control problems in aircraft dynamics, in particular, the dynamics of an unmanned aerial system (UAS), it is frequently useful to analyze the way of defining the kinematic and dynamic parameters.

Unlike the traditional representation of a motion in terms of decoupled translation and rotation, Gulio Mozzi proved in 1763 that any general rigid body motion can be described by an instantaneous screw axis (ISA) [3, 4]. One of the applications of the ISM concept in rigid body kinematics is the invariant description of rigid body motion that is presented by J. Schutter [2].

This research aims to analyze the instantaneous screw motion (ISM) concept in UAS dynamics, control, guidance. Figure 1.1 shows the steps towards the implementation of this goal. First of all, the ISM concept is analyzed by determining the expressions for the invariants and deriving the equations of motion of the instantaneous screw axis (ISA). Second, the relationship between the flight dynamics and the ISM invariants will be established. Third, the relationship between the invariants and the control parameters will be studied. The proposed GNC algorithm with ISM invariants is described in Figure 1.2. The future works will include creating novel explicit guidance and navigation techniques based on the ISM invariants [5].

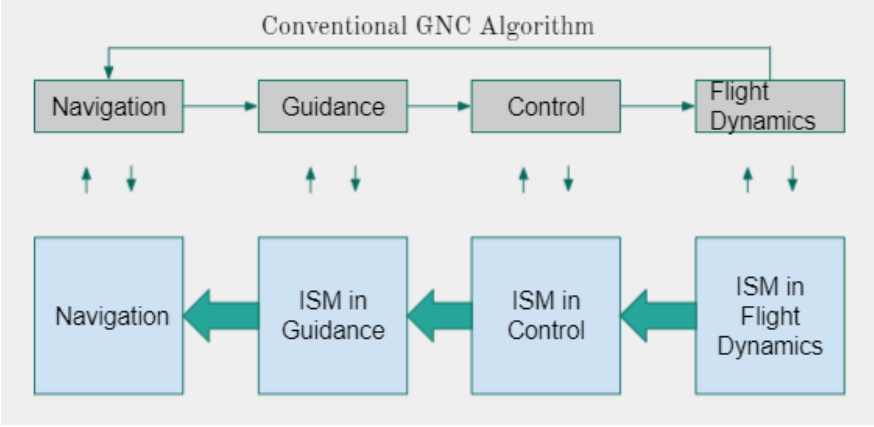

Figure 1.1: Conventional GNC Loop and ISM-based Approach

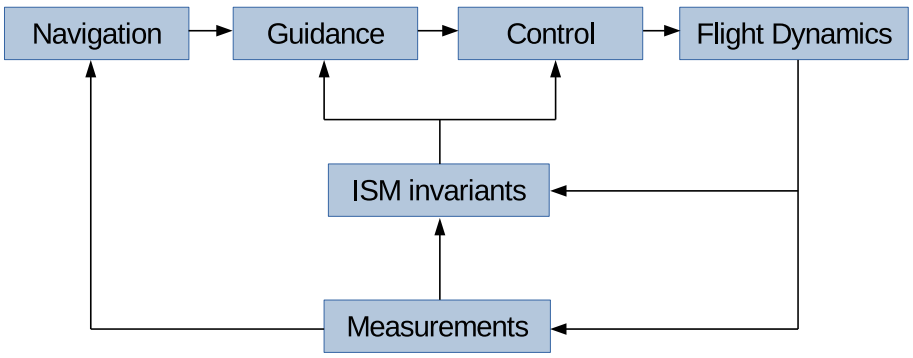

Figure 1.2: Proposed GNC system with ISM invariants

1.2 Literature Review

Over the course of the last two decades, the demand for unmanned aerial vehicles (UAVs) has increased significantly. The main reason for that is their capability to carry out an impressive range of tasks, ranging from taking photos to military operations. Today, we can find numerous works devoted to the development of UAVs, and they can be primarily divided into three groups: autonomy, path planning, and optimality.

One group of works is devoted to the quadcopter, its dynamics, and control. It has been shown that the quadcopter dynamics can be defined mathematically by using Newton-Euler, Euler-Lagrange equations and physical aspects of motion [6],[7]. Moreover, considerable simulation results have been obtained by integrating control systems like PD controllers [6]-[8]. Mathematic and dynamic models of the quadcopter, control, and guidance problems for it have been studied and considerable results are obtained [9].

The most common way of defining a rigid body motion is the traditional method of decoupled translational and rotational motions. It is shown that when considering the UAV dynamics and problems it is useful to consider the coordinate systems along with the way of defining the motion. One of the methods of describing the motion is the utility of a concept of an instantaneous screw axis (ISA). Any rigid body motion can be defined via the concept of the ISA [3, 4, 10]. Utilizing the ISA is potentially useful to compute the control functions and/or decrease the error in controlling. J. Angeles studied the problem of computing the screw parameters of rigid-body motion for finitely-separated positions [11]. The second part of his work studies the same problem for infinitesimally-separated positions [12]. Based on the survey of the existing studies, one can conclude that the concept of the ISA is new in the analysis of the UAV guidance, navigation, and control problems. In the following paragraphs, some of the works that addressed the UAVs are described.

A large group of studies focuses on UAV autonomy. The importance of autonomous UAVs, the

current and future demand for them was explained in detail in Ref. [13],[14]. One example deals with the problem of how to design and integrate autonomous systems into existing and new vehicles. A modular system architecture was proposed that will enable the safe and trustworthy performance of multiple-scenario missions [14]. Sense and Avoid (S&A) system has also been studied thoroughly, and some future directions of development of autonomous S&A system were presented in Ref. [15]. Lee *et. al* described the tracking guidance for the autonomous UAV landing and vision-based detection of the marker on the moving vehicle with the real-time image processing system [16]. The problem of UAV navigation in a GPS denied environment was addressed by one research work [17]. G. Rudnick *et. al* described a concept for scalable autonomy of UAVs applicable to the field of reconnaissance missions [18]. C. Rogers *et. al* presented a modular heterogeneous multi-agent control framework with payload integration, which provides a wireless network between agents without relying on pre-existing communication infrastructure [19]. Moreover, a novel approach to estimate the relative position of an aircraft that is connected to a fixed location on the ground through a taut tether of varying length was presented [20]. Besides that, a novel decentralized task allocation algorithm based on the Hungarian approach was proposed in one work [21].

A group of works presents path planning and guidance for UAVs [22, 23, 24, 25, 26]. For example, for fixed-wing UAVs with a finite field of view, a cooperative track-before-detect algorithm for multiple ground targets was described in one of these works [23]. P. Maini *et. al* defined a two-step path planning algorithm for UAVs with kinematic constraints in the presence of polygonal obstacles [24]. M. Beul *et. al* proposes a novel trajectory generation method that is able to compute time and energy-optimal trajectories analytically for micro aerial vehicles [25]. A path planning method for UAVs surveying a cluttered urban landscape was presented in Ref. [27]. In addition, a pathfinding method for two UAVs with localization constraints was proposed using a modified shortest path algorithm [28]. T. Andersen *et. al* proposes a quaternion-based guidance law and addresses the problem of trajectory tracking for underactuated quadrotors [29]. E. Kawamura showed the integration of targeting, guidance, control and navigation functions for real-time implementation onboard UAVs [30]. For a vertical plane (fixed-wing UAV), an analytical model of dynamics was obtained, and it is particularly very useful to develop guidance and control solutions [31]. In addition, a nonlinear landing-guidance law was developed using the sliding-mode control scheme for UAVs to land on carriers at sea [32]. An improved path-following performance for fixed-wing UAVs, considering the wind velocity, was proposed [33]. D'Amato *et. al* studied this problem in complex 3D environments, taking both mission and aircraft performance constraints into account [34]. A decentralized method to generate collision-free 3D trajectories for UAVs flying in a shared space was proposed in Ref.[35]. Ya Liu *et. al* analyzed cooperative transportation of tethered multi-rotor UAVs, and proposed an optimized trajectory to accomplish the payload manipulation [36]. Moreover, a highly feasible trajectory planning method for control-oriented UAVs was proposed in Ref [37]. Furthermore, various guidance laws and techniques have been developed

by employing the quartic polynomial, Lyapunov's second method, the v-nulling method, the vision-based and other numerical methods, approximate and analytical methods, regardless of the control actuation devices [26], [23]-[36].

Another group of studies deals with the problems of optimality [38, 39]. A.A. Munishkin *et. al* considers two nonholonomic vehicles, of which one has the goal to enter the "tail" of the other. Since the goal and navigation strategy of the second vehicle are unknown, the first vehicle uses infinite horizon stochastic optimal control [38]. A. Matus-Vargas *et. al* studied the use of two optimization techniques for coefficient tuning when the dynamic model is nonlinear [39].

1.3 Overview of Chapters and Appendices

Chapter 2 deals with UASs in the example of quadcopter and fixed-wing UAV. Dynamic models and equations of motion of the quadcopter and fixed-wing UAVs are provided. Chapter 3 provides a deep study of the ISM concept including the motion of the ISA. Analysis of the ISM invariant in the motion of the quadcopter is discussed in Chapter 4. In Chapter 5, the invariants are studied in the fixed-wing dynamics. Chapter 7 provides the conclusions and future works. Appendix A provides the expression for the 6th invariant, while Appendix B includes the scalar forms of i_4 and i_6 (invariant 4 and 6). Appendix C provides the list of journal papers and seminars.

CHAPTER 2
UNMANNED AERIAL SYSTEMS

2.1 Quadcopter Dynamic Model

2.1.1 Kinematics

The general motion of a rigid body can be defined as the combination of the translational motion of a point from the rigid body and the rigid body's rotational motion about the coordinate axes. One of the ways of defining the rotational motion is using the Euler angles which can be determined using two frames: inertial and body frames. The inertial frame is fixed on the ground and defined by x, y, z - axes, while the body frame is fixed on the rigid body and defined by x_B, y_B, z_B - axes. In order to define the quadcopter's motion, we use these two frames. In this case, the center of mass is considered to be the reference point and the body frame is fixed at this point [6].

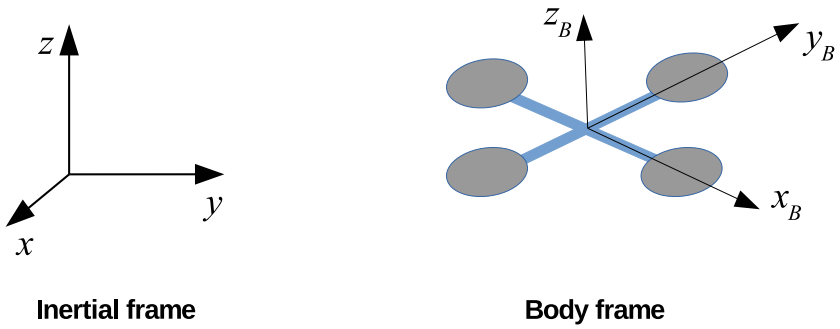

Figure 2.1: Inertial and Body frames

The linear position and velocity vectors (denoted by $\boldsymbol{\xi}$ and $\boldsymbol{\eta}$ respectively) of the quadcopter in the inertial frame can be defined as

$$\boldsymbol{\xi} = \begin{bmatrix} x \\ y \\ z \end{bmatrix}, \quad \dot{\boldsymbol{\xi}} = \begin{bmatrix} \dot{x} \\ \dot{y} \\ \dot{z} \end{bmatrix}. \tag{2.1}$$

The angular position and velocity vectors are defined through the Euler angles as

$$\boldsymbol{\eta} = \begin{bmatrix} \phi \\ \theta \\ \psi \end{bmatrix}, \quad \boldsymbol{\omega} = \boldsymbol{W^{-1}}\dot{\boldsymbol{\eta}} = \begin{bmatrix} 1 & 0 & -sin\ \theta \\ 0 & cos\ \phi & cos\theta\ sin\phi \\ 0 & -sin\ \phi & cos\theta\ cos\phi \end{bmatrix} \begin{bmatrix} \dot{\phi} \\ \dot{\theta} \\ \dot{\psi} \end{bmatrix}, \tag{2.2}$$

where $\boldsymbol{W}$ is the transformation matrix for angular velocities from the inertial frame to the body frame [40]. The rotation matrix for the position and other vectors from the body frame to the inertial frame is given as [6]

$$\boldsymbol{R} = \begin{bmatrix} cos\psi cos\theta & cos\psi sin\theta sin\phi - sin\psi cos\phi & cos\psi sin\theta cos\phi + sin\psi sin\phi \\ sin\psi cos\theta & sin\psi sin\theta sin\phi - cos\psi cos\phi & sin\psi sin\theta cos\phi + cos\psi sin\phi \\ -sin\theta & cos\theta sin\phi & cos\theta cos\phi \end{bmatrix}. \tag{2.3}$$

2.1.2 Forces and Torques

Forces

There are gravity $\boldsymbol{G}$, thrust $\boldsymbol{T^B}$ from the rotors, and aerodynamic drag $\boldsymbol{D}$ forces acting on the quadcopter. The gravity in the inertial frame is given as

$$\boldsymbol{G} = \begin{bmatrix} 0 \\ 0 \\ -mg \end{bmatrix}, \tag{2.4}$$

where m is the mass of the quadcopter, g is gravitational acceleration.
The thrust from the rotors can be defined in the body frame as

$$\boldsymbol{T^B} = \begin{bmatrix} 0 \\ 0 \\ T \end{bmatrix}, \tag{2.5}$$

where T is the sum of the thrusts from four rotors, and it is given by

$$T = k \sum_{1}^{4} \omega_i^2, \tag{2.6}$$

where k is the lift constant, ω_i is the angular rate of ith rotor [7].
The thrust in the inertial frame is determined by

$$\boldsymbol{T^I} = \boldsymbol{R}\boldsymbol{T^B}.$$

From the fluid dynamics, the drag force is given by the following equation

$$D = \frac{1}{2}\rho C_D A v^2, \tag{2.7}$$

where ρ is the surrounding fluid density, v is the velocity of the surrounding fluid, A is the reference area, and C_D is drag constant [41]. The drag constant can be determined from the experiment, and

it depends on the shape of the object and Reynolds number. Figure 2.2 shows Reynolds numbers for small UAVs [1]. At low Reynolds numbers, the drag coefficient is asymptotically proportional to

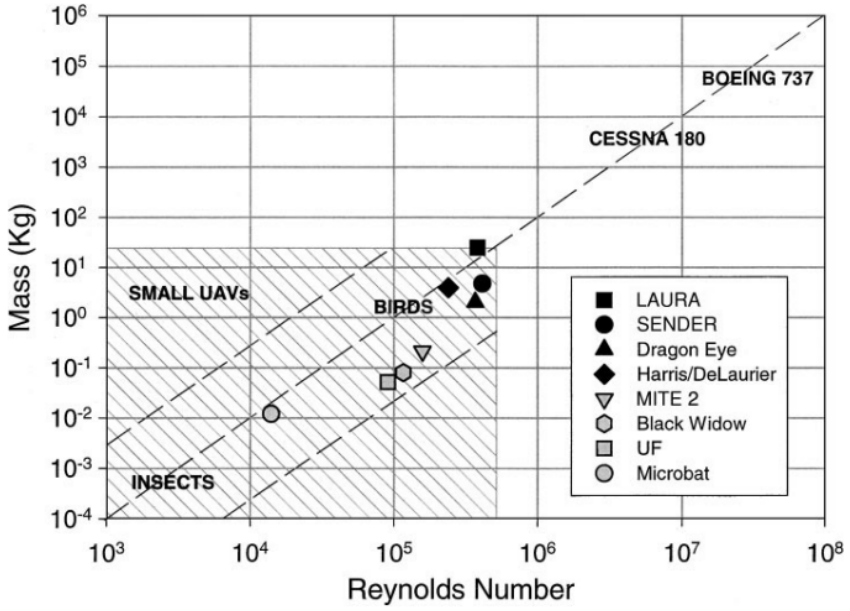

Figure 2.2: Reynolds number for Small UAVs [1]

R_e^{-1}, which means that the drag is linearly proportional to the velocity. At high Reynolds numbers, the drag would be proportional to the square of the velocity [42].

The linear model of the drag was proposed and considered in several studies on the quadcopter [6, 7, 43, 44]. For example, Bouadi *et. al* and Derafa *et. al* considered the drag to be proportional to the velocity with different coefficients in each direction [43, 44]. In another study, the linear drag was modeled with the same coefficient in every direction [7]. For simplicity purposes, the linear model of the drag is chosen and considered in this paper. Thus, it can be defined in the inertial frame as

$$\boldsymbol{D} = -k_d \begin{bmatrix} \dot{x} \\ \dot{y} \\ \dot{z} \end{bmatrix}, \tag{2.8}$$

where k_d - drag constant.

In this model, the drag force for the rotational motion is assumed to be negligible in the case of relatively small angular velocities.

Torques

The total torques about the x and y axes in the body frame can be found as the functions of angular rates of the rotors depending on the fixed state of the body frame. Assuming that the rotors 1 and

3 are located on the y axis of the body frame, we can write the roll and pitch torques as

$$\begin{aligned}\tau_\phi &= lk(\omega_1^2 - \omega_3^2),\\ \tau_\theta &= lk(\omega_2^2 - \omega_4^2),\end{aligned} \tag{2.9}$$

where l is the distance between the rotor and the center of the quadcopter.
Using the expression for the frictional force in the fluid dynamics, the torque about the z axis can be written in the following form assuming the angular acceleration to be zero (or negligible):

$$\tau_\psi = b_\tau(\omega_1^2 - \omega_2^2 + \omega_3^2 - \omega_4^2), \tag{2.10}$$

where b_τ is torque drag coefficient [7].
So, the total torque in the body frame is given by

$$\boldsymbol{\tau_B} = \begin{bmatrix}\tau_\phi\\ \tau_\theta\\ \tau_\psi\end{bmatrix} = \begin{bmatrix} lk(\omega_1^2 - \omega_3^2)\\ lk(\omega_2^2 - \omega_4^2)\\ b_\tau(\omega_1^2 - \omega_2^2 + \omega_3^2 - \omega_4^2)\end{bmatrix}. \tag{2.11}$$

2.1.3 Equations of Motion

The equations of motion consist of two parts: the equations for the linear motion and the equations for the rotational motion. The linear equations of motion can be derived using the Newton's second law as

$$m\ddot{\boldsymbol{\xi}} = \boldsymbol{G} + \boldsymbol{RT^B} + \boldsymbol{D} \tag{2.12}$$

The equations for the rotational motion can be derived from the Euler's equation below

$$\boldsymbol{I}\dot{\boldsymbol{\omega}} + \boldsymbol{\omega} \times (\boldsymbol{I}\boldsymbol{\omega}) = \boldsymbol{\tau}, \tag{2.13}$$

where $\boldsymbol{I}$ is inertia matrix, ω is angular velocity vector, $\boldsymbol{\tau}$ - total external torque vector [7]. It is assumed that the quadcopter has a symmetric structure with two thin uniform rods crossed at the center. Therefore, the inertia matrix can be written as a diagonal matrix as

$$\boldsymbol{I} = \begin{bmatrix} I_{xx} & 0 & 0\\ 0 & I_{yy} & 0\\ 0 & 0 & I_{zz}\end{bmatrix}. \tag{2.14}$$

Substituting the Eqs. (2.11) and (2.14) into Eq. (2.13), the following equation can be taken for the rotational motion:

$$\begin{bmatrix} I_{xx} & 0 & 0 \\ 0 & I_{yy} & 0 \\ 0 & 0 & I_{zz} \end{bmatrix} \begin{bmatrix} \dot{\omega}_x \\ \dot{\omega}_y \\ \dot{\omega}_z \end{bmatrix} + \begin{bmatrix} \omega_x \\ \omega_y \\ \omega_z \end{bmatrix} \times \begin{bmatrix} I_{xx} & 0 & 0 \\ 0 & I_{yy} & 0 \\ 0 & 0 & I_{zz} \end{bmatrix} \begin{bmatrix} \omega_x \\ \omega_y \\ \omega_z \end{bmatrix} = \begin{bmatrix} \tau_\phi \\ \tau_\theta \\ \tau_\psi \end{bmatrix}, \tag{2.15}$$

or

$$\begin{bmatrix} \dot{\omega}_x \\ \dot{\omega}_y \\ \dot{\omega}_z \end{bmatrix} = \begin{bmatrix} \tau_\phi I_{xx}^{-1} \\ \tau_\theta I_{yy}^{-1} \\ \tau_\psi I_{zz}^{-1} \end{bmatrix} - \begin{bmatrix} \frac{I_{yy}-I_{zz}}{I_{xx}} \omega_y \omega_z \\ \frac{I_{zz}-I_{xx}}{I_{yy}} \omega_x \omega_z \\ \frac{I_{xx}-I_{yy}}{I_{zz}} \omega_y \omega_x \end{bmatrix}. \tag{2.16}$$

where $\omega_x,\ \omega_y,\ \omega_z$ - angular velocity vector components.

2.2 Fixed-wing UAV Dynamic Model

2.2.1 Equations of Motion

Similar to the quadcopter's kinematics, the equations of motion of a fixed-wing aircraft can be defined using two frames: the inertial frame and the body frame. The inertial frame is fixed on the ground at sea level and denoted as $Exyh$. The body frame is denoted $Be_1e_2e_3$ and fixed on the aircraft's center of gravity (COG) with the velocity vector pointing in e_1-direction. If the sideslip angle is zero (i.e $\beta = 0$) and the bank angle is constant (i.e $\phi = \phi_0$), then the atmospheric flight equations can be obtained as

$$\begin{aligned} \dot{x} &= v\ cos\ \gamma\ cos\ \psi, \\ \dot{y} &= v\ cos\ \gamma\ sin\ \psi, \\ \dot{h} &= v\ sin\ \gamma, \\ \dot{v} &= \frac{g_0}{m}(T\ cos\ \alpha - D) - g_0\ sin\ \gamma, \\ \dot{\gamma} &= \frac{g_0}{W\ v}(T\ sin\ \alpha + L) - \frac{g_0}{v}\ cos\ \gamma, \\ \dot{\psi} &= \frac{g_0}{W\ v\ cos\ \gamma}(T\ sin\ \alpha + L) sin\ \phi_0, \\ \dot{W} &= -CT, \end{aligned} \tag{2.17}$$

where v - velocity magnitude, γ - flight path angle, ψ - heading angle, ϕ_0 - bank angle, g_0 - magnitude of gravitational acceleration, T - thrust, L - lift, D - drag, W - weight, C - specific fuel consumption [45].

The lift and drag forces are defined to be the components of the resultant aerodynamic force

perpendicular and parallel to the velocity vector:

$$L = \frac{1}{2} C_L \rho S v^2, \quad D = \frac{1}{2} C_D \rho S v^2, \tag{2.18}$$

where $C_L,\ C_D$ - lift and drag coefficients, ρ - the density of the atmosphere at the altitude of the aircraft, and S is the wing platform area [45].
Considering the following expressions constant allows calculating the propulsive thrust and angle of attack as well as making the equations of motion integrable analytically

$$\frac{g_0}{W}(T\ cos\ \alpha - D) = c_1, \quad \frac{g_0}{W}(T\ sin\ \alpha + L) = c_2, \tag{2.19}$$
$$c_1,\ c_2 - const.$$

This assumption was validated by demonstrating that the values of the thrust and angle of attack obtained for various values of lift, weight, and power settings are within the existing ranges for certain types of aircrafts. It has also been proved that these assumptions can be valid for an aircraft with high maneuverability [46, 31].
Assuming that the change of the weight is negligible, Eqs.(2.17) can be rewritten in the following form [31, 46]

$$\begin{aligned}
\dot{x} &= v\ cos\ \gamma\ cos\ \psi, \\
\dot{y} &= v\ cos\ \gamma\ sin\ \psi, \\
\dot{h} &= v\ sin\ \psi, \\
\dot{v} &= c_1 - g_0\ sin\ \gamma, \\
\dot{\gamma} &= \frac{1}{v}(c_2 cos\phi_0 - g_0)\ cos\ \gamma, \\
\dot{\psi} &= \frac{c_2\ sin\ \phi_0}{v\ cos\ \gamma}.
\end{aligned} \tag{2.20}$$

The integrals of Eqs.(2.20) are obtained in terms of γ, assuming that γ is an independent variable:

$$
\begin{aligned}
x(\gamma) &= \int \frac{v^2(\lambda) sin\ \lambda\ cos\ \psi \mathrm{d}\lambda}{a + b\ sin\ \lambda} + \eta_1, \\
y(\gamma) &= \int \frac{v^2(\lambda) sin\ \lambda\ sin\ \psi \mathrm{d}\lambda}{a + b\ sin\ \lambda} + \eta_2, \\
h(\gamma) &= Q(\gamma) exp\left[\frac{4A}{d_1} arctan \frac{a\ tan\ \bar{\lambda} + b}{d_1}\right] + \eta_3, \\
v(\gamma) &= \eta_4 (a + b\ sin\ \lambda)^{-1} exp\left[\frac{2A}{d_1} arctan \frac{a\ tan\ \bar{\lambda} + b}{d_1}\right], \\
\psi(\gamma) &= tan\ \phi_0\ ln(tan\ \bar{\lambda}) + \frac{2g_0}{d_1} tan\ \phi_0\ arctan\left(\frac{a\ tan\ \bar{\lambda} + b}{d_1}\right) + \eta_5,
\end{aligned}
\tag{2.21}
$$

where η_{1-5}, A - integration constants, $a = c_2 cos\ \phi_0$, $b = -g_0$, $\lambda = \gamma + \frac{\pi}{2}$, $\bar{\lambda} = \lambda/2$, $Q(\gamma)$ - function of γ [46].
For simplicity purposes, the heading angle will be considered constant, i.e the motion is in a vertical plane.

2.2.2 Control Parameters

Thrust and angle of attack are the control parameters, and they can be found from Eqs.(2.19). For small angles of attack [31]

$$
\alpha_{1,2} = \frac{1}{2g_1}\left(\sqrt{g_2^2 - 4g_1 g_3} - g_2\right), \tag{2.22}
$$

where

$$
\begin{aligned}
g_1(h, v) &= \frac{1}{2} k \rho S v^2 C_{L\alpha}^2 (2\alpha_{0L} + \alpha_T), \\
g_2(h, v) &= mc_1 + \frac{1}{2}\rho S v^2 (C_{D0} + K C_{L\alpha}^2 \alpha_{0L}^2 + 2K C_{L\alpha}^2 \alpha_{0L} \alpha_T + C_{L\alpha}), \\
g_3(h, v) &= m(c_1 \alpha_T - c_2) + \frac{1}{2}\rho S v^2 (C_{D0} + K C_{L\alpha}^2 \alpha_{0L}^2 \alpha_T + C_{L\alpha} \alpha_{0L}),
\end{aligned}
\tag{2.23}
$$

k - const, α_{0L} - zero-lift angle of attack, α_T - angle between thrust and body axis, C_{D0}, K - coefficients of drag polar, m - mass, $C_{L\alpha}$ - lift-curve slope of the wing.
If the air density is considered constant, then the expressions above can be simplified. By intro-

ducing the following notations

$$
\begin{aligned}
q_1 &= \frac{1}{2}k\rho S C_{L\alpha}^2(2\alpha_{0L} + \alpha_T),\\
q_2 &= mc_1,\\
q_3 &= \frac{1}{2}\rho S(C_{D0} + KC_{L\alpha}^2\alpha_{0L}^2 + 2KC_{L\alpha}^2\alpha_{0L}\alpha_T + C_{L\alpha}cos\phi),\\
q_4 &= m(c_1\alpha_T - c_2),\\
q_5 &= \frac{1}{2}\rho S(C_{D0} + KC_{L\alpha}^2\alpha_{0L}^2\alpha_T + C_{L\alpha}\alpha_{0L}cos\phi),
\end{aligned}
\tag{2.24}
$$

where q_i - constants, Eqs.(2.23) can be rewritten as

$$
\begin{aligned}
g_1(v) &= q_1v^2,\\
g_2(v) &= q_2 + q_3v^2,\\
g_3(v) &= q_4 + q_5v^2.
\end{aligned}
\tag{2.25}
$$

After substituting these equations into Eq.(2.22) and solving for v, one can get

$$
v(\alpha) = \sqrt{\frac{q_1q_2\alpha - q_1q_4}{q_1^2\alpha^2 + q_1q_3\alpha - q_1q_5}},
\tag{2.26}
$$

where v is always positive. The expression for thrust can be obtained as [31]

$$
T = \sqrt{(mc_1 + D)^2 + (mc_2 - L)^2},
\tag{2.27}
$$

or

$$
T(\alpha) = \sqrt{(mc_1 + \frac{1}{2}C_D\rho_\alpha Sv_\alpha^2)^2 + (mc_2 - \frac{1}{2}C_L\rho_\alpha Sv_\alpha^2)^2},
\tag{2.28}
$$

where $v_\alpha = v(\alpha)$.

CHAPTER 3
INSTANTANEOUS SCREW MOTION INVARIANTS

3.1 Description of Invariants

Using Schutter's work on defining the rigid body motion instantaneously, in this section the invariant description of rigid body motion will be represented [2]. The screw motion of the rigid body is defined by two parameters: the rotational velocity of the rigid body about the screw axis, and the translational velocity of the rigid body along the screw axis. In the case of general motion of the rigid body, the translational and rotational velocity vectors cannot be considered as constants, and therefore the state of the screw axis changes as these two vectors change. The rigid body motion can be defined by six invariants. The first two invariants are the two parameters of the instantaneous screw motion (ISM) of the rigid body. The other four invariants define the motion of the screw axis.

Invariants:

$i_1 = \omega_1(t)$ - rotational velocity about the instantaneous screw axis (ISA);

$i_2 = v_1(t)$ - translational velocity along the ISA;

$i_3 = \omega_2(t)$ - rotational velocity of the ISA about $y(t - \Delta t)$-axis;

$i_4 = v_2(t)$ - translational velocity of the ISA along $y(t - \Delta t)$-axis;

$i_5 = \omega_3(t)$ - rotational velocity of the frame attached to the ISA about $x(t)$-axis;

$i_6 = v_3(t)$ - translational velocity of the frame attached to the ISA along $x(t)$-axis.

3.2 Derivation of Invariants

If $\boldsymbol{\omega}$ and $\boldsymbol{v}$ are the rotational and translational velocity vectors of the rigid body, then

$$\boldsymbol{e_x} = \frac{\boldsymbol{\omega}}{\|\boldsymbol{\omega}\|},\ \omega_1 = \|\boldsymbol{\omega}\| = \boldsymbol{\omega} \cdot \boldsymbol{e_x}, \tag{3.1}$$

$$v_1 = \boldsymbol{v} \cdot \boldsymbol{e_x} = \frac{\boldsymbol{v} \cdot \boldsymbol{\omega}}{\|\boldsymbol{\omega}\|}, \tag{3.2}$$

where $\boldsymbol{e_x}$ is the unit vector along the ISA. The following equations can be written from the Fig. 3.1a:

$$\omega_2(t) = \lim_{\Delta t \to 0} \frac{\Delta \theta_2(t)}{\Delta t}, \tag{3.3}$$

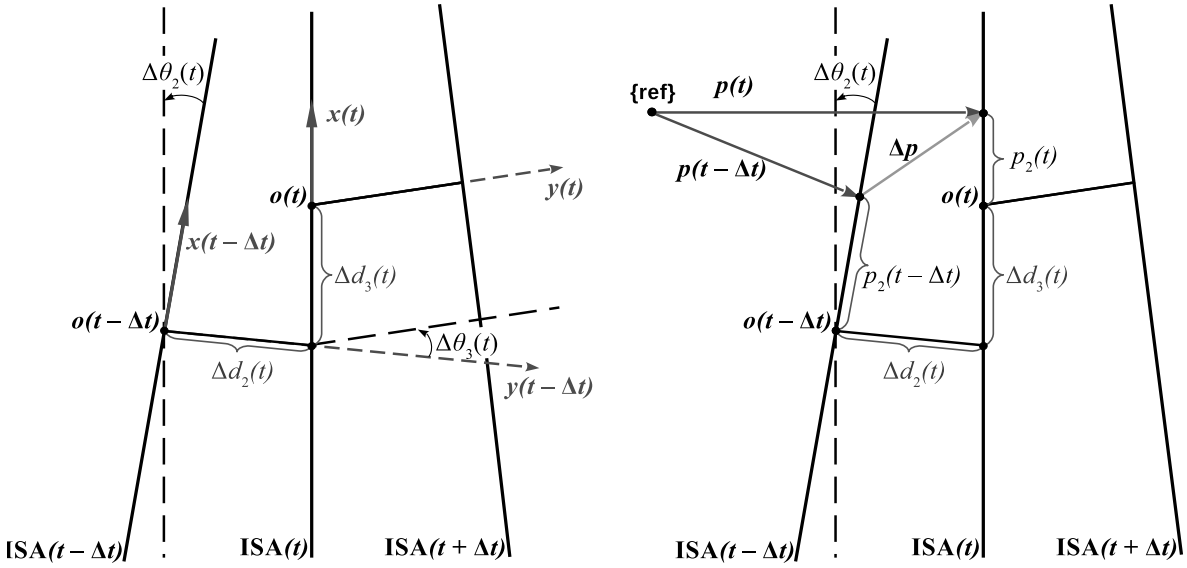

(a) (b)

Figure 3.1: ISA in three consecutive time instants [2]

$$v_2(t) = \lim_{\Delta t \to 0} \frac{\Delta d_2(t)}{\Delta t}, \tag{3.4}$$

$$\omega_3(t) = \lim_{\Delta t \to 0} \frac{\Delta \theta_3(t)}{\Delta t}, \tag{3.5}$$

$$v_3(t) = \lim_{\Delta t \to 0} \frac{\Delta d_3(t)}{\Delta t}. \tag{3.6}$$

Since $\boldsymbol{\omega}$ vector and the ISA are always parallel, the rotation of $\boldsymbol{\omega}$ can be considered to find the rotation of the ISA. It is known that (see Fig. 3.2b)

$$\Delta\theta_2 = \frac{\|\dot{\boldsymbol{\omega}}\| sin\alpha \cdot \Delta t}{\|\boldsymbol{\omega}\|}. \tag{3.7}$$

Using

$$\|\boldsymbol{\omega} \times \dot{\boldsymbol{\omega}}\| = \|\boldsymbol{\omega}\| \|\dot{\boldsymbol{\omega}}\| sin\alpha, \tag{3.8}$$

the Eq. (3.7) can be rewritten as

$$\Delta\theta_2 = \frac{\|\boldsymbol{\omega} \times \dot{\boldsymbol{\omega}}\| \cdot \Delta t}{\|\boldsymbol{\omega}\|^2}. \tag{3.9}$$

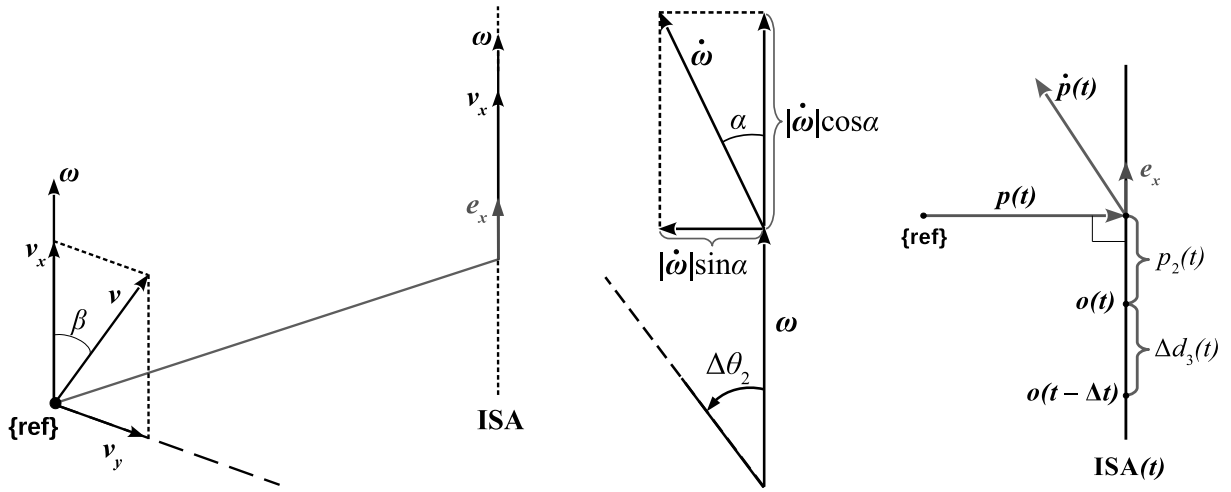

(a) (b) (c)

Figure 3.2: Screw parameters

By substituting Eq. (3.9) into Eq. (3.3), the following equation can be obtained

$$\omega_2 = \lim_{\Delta t \to 0} \frac{\|\boldsymbol{\omega} \times \dot{\boldsymbol{\omega}}\| \cdot \Delta t}{\|\boldsymbol{\omega}\|^2 \cdot \Delta t} = \frac{\|\boldsymbol{\omega} \times \dot{\boldsymbol{\omega}}\|}{\|\boldsymbol{\omega}\|^2}. \tag{3.10}$$

In order to find v_2, $\boldsymbol{p}$ - position vector, originating from the origin of {ref} and perpendicular to the ISA, is used (Fig. 3.1b).
It is seen from Fig. 3.2a that the velocity vector $\boldsymbol{v}$ can be expressed as the geometric sum of $\boldsymbol{v_x}$ and $\boldsymbol{v_y}$ vectors:

$$\boldsymbol{v} = \boldsymbol{v_x} + \boldsymbol{v_y}, \tag{3.11}$$

where

$$\boldsymbol{v_x} = v_1 \cdot \boldsymbol{e_x} = \frac{\boldsymbol{\omega}}{\|\boldsymbol{\omega}\|} v_1, \ \boldsymbol{v} = \boldsymbol{\omega} \times \boldsymbol{r}. \tag{3.12}$$

The latter equation is for a rotational motion, it can be used to find $\boldsymbol{v_y}$:

$$\boldsymbol{v_y} = \boldsymbol{\omega} \times (-\boldsymbol{p}) = \boldsymbol{p} \times \boldsymbol{\omega}. \tag{3.13}$$

Eq. (3.11) can be rewritten as

$$\boldsymbol{v} = \frac{\boldsymbol{\omega}}{\|\boldsymbol{\omega}\|} v_1 + \boldsymbol{p} \times \boldsymbol{\omega}, \tag{3.14}$$

hence

$$\boldsymbol{\omega} \times \boldsymbol{v} = \frac{\boldsymbol{\omega} \times \boldsymbol{\omega}}{\|\boldsymbol{\omega}\|} v_1 + \boldsymbol{\omega} \times (\boldsymbol{p} \times \boldsymbol{\omega}), \tag{3.15}$$

from which one can obtain

$$\boldsymbol{\omega} \times \boldsymbol{v} = \|\boldsymbol{\omega}\|^2 \boldsymbol{p}, \ \boldsymbol{p} = \frac{\boldsymbol{\omega} \times \boldsymbol{v}}{\|\boldsymbol{\omega}\|^2}. \tag{3.16}$$

Now, one can calculate the time derivative of $\boldsymbol{p}$ as

$$\dot{\boldsymbol{p}} = \frac{(\dot{\boldsymbol{\omega}} \times \boldsymbol{v} + \boldsymbol{\omega} \times \dot{\boldsymbol{v}}) \cdot \|\boldsymbol{\omega}\|^2 - 2(\boldsymbol{\omega} \times \boldsymbol{v}) \cdot (\boldsymbol{\omega} \cdot \dot{\boldsymbol{\omega}})}{\|\boldsymbol{\omega}\|^4}, \tag{3.17}$$

and v_2 is computed by projecting $\dot{\boldsymbol{p}}$ onto the y-axis:

$$v_2 = \boldsymbol{e_y} \cdot \dot{\boldsymbol{p}}, \tag{3.18}$$

where $\boldsymbol{e_y}$ is the unit vector along the y-axis. Since the y-axis is perpendicular to $\boldsymbol{\omega}$ and $\dot{\boldsymbol{\omega}}$, the unit vector $\boldsymbol{e_y}$ is computed as

$$\boldsymbol{e_y} = \frac{\boldsymbol{\omega} \times \dot{\boldsymbol{\omega}}}{\|\boldsymbol{\omega} \times \dot{\boldsymbol{\omega}}\|}, \tag{3.19}$$

and therefore Eq. (3.18) can be rewritten as

$$v_2 = \frac{\boldsymbol{\omega} \times \dot{\boldsymbol{\omega}}}{\|\boldsymbol{\omega} \times \dot{\boldsymbol{\omega}}\|} \cdot \dot{\boldsymbol{p}} \, . \tag{3.20}$$

ω_3 is found in a similar way as ω_2 (see Eq. (3.10)). In this case $\omega_2 \cdot \boldsymbol{e_y}$ can be used instead of $\boldsymbol{\omega}$:

$$\omega_2 \cdot \boldsymbol{e_y} = \frac{\boldsymbol{\omega} \times \dot{\boldsymbol{\omega}}}{\|\boldsymbol{\omega}\|^2}, \tag{3.21}$$

$$\omega_3 = \frac{\|(\omega_2 \cdot \boldsymbol{e_y}) \times \frac{d}{dt}(\omega_2 \cdot \boldsymbol{e_y})\|}{\|\omega_2 \cdot \boldsymbol{e_y}\|^2} = \frac{\|(\boldsymbol{\omega} \times \dot{\boldsymbol{\omega}}) \times (\boldsymbol{\omega} \times \ddot{\boldsymbol{\omega}})\|}{\|\boldsymbol{\omega} \times \dot{\boldsymbol{\omega}}\|^2} \tag{3.22}$$

The derivation of v_3 involves two steps.
1) The angular velocity of the ISA is directed perpendicular to xz-plane, and its value is equal to ω_2. From Eq. (3.14),

$$\dot{\boldsymbol{p}}_{\boldsymbol{z}} = (\omega_2 \cdot \boldsymbol{e_y}) \times (p_2 \cdot \boldsymbol{e_x}) \tag{3.23}$$

where $\dot{\boldsymbol{p}}_{\boldsymbol{z}} = (\dot{\boldsymbol{p}} \cdot \boldsymbol{e_z}) \cdot \boldsymbol{e_z}$ - the component of $\dot{\boldsymbol{p}}$ on z-axis, p_2 - the distance between the central point of the ISA and the intersection point of it with the position vector. From Eq.(3.23), it can be found that

$$\|\dot{\boldsymbol{p}}_{\boldsymbol{z}}\| = \|\omega_2 \cdot \boldsymbol{e_y}\| \cdot \|p_2 \cdot \boldsymbol{e_x}\| \tag{3.24}$$

from which

$$p_2 = -\frac{\dot{\boldsymbol{p}} \cdot \boldsymbol{e_z}}{\omega_2} \tag{3.25}$$

where

$$\boldsymbol{e_z} = \boldsymbol{e_x} \times \boldsymbol{e_y} = \frac{\boldsymbol{\omega} \times (\boldsymbol{\omega} \times \dot{\boldsymbol{\omega}})}{\|\boldsymbol{\omega}\| \cdot \|\boldsymbol{\omega} \times \dot{\boldsymbol{\omega}}\|}. \tag{3.26}$$

2) Since the motion is instantaneous, the velocities should be considered rather than distances or angles changed. From Fig. 3.2c it can be seen that

$$\Delta d_3 = (\dot{\boldsymbol{p}} \cdot \boldsymbol{e_x}) \cdot \Delta t - \dot{p}_2 \cdot \Delta t. \tag{3.27}$$

Substituting Eq. (3.27) into Eq. (3.6) yields

$$v_3 = \lim_{\Delta t \to 0} \frac{(\dot{\boldsymbol{p}} \cdot \boldsymbol{e_x}) \cdot \Delta t - \dot{p}_2 \cdot \Delta t}{\Delta t} = \dot{\boldsymbol{p}} \cdot \boldsymbol{e_x} - \dot{p}_2. \tag{3.28}$$

After calculation, an expression for v_3 can be obtained as $v_3 = v_3(\boldsymbol{\omega}, \dot{\boldsymbol{\omega}}, \ddot{\boldsymbol{\omega}}, \boldsymbol{v}, \dot{\boldsymbol{v}}, \ddot{\boldsymbol{v}})$. The resulting expression for v_3 is given in Appendix A.

In summary, the expressions for the invariants can be written as

$$\begin{aligned}
i_1 &= i_1(\boldsymbol{\omega}) = \boldsymbol{\omega} \cdot \boldsymbol{e_x} = \|\boldsymbol{\omega}\|, \\
i_2 &= i_2(\boldsymbol{v}, \boldsymbol{\omega}) = \boldsymbol{v} \cdot \boldsymbol{e_x} = \frac{\boldsymbol{v} \cdot \boldsymbol{\omega}}{\|\boldsymbol{\omega}\|}, \\
i_3 &= i_3(\boldsymbol{\omega}, \dot{\boldsymbol{\omega}}) = \frac{\boldsymbol{\omega} \times \dot{\boldsymbol{\omega}}}{\|\boldsymbol{\omega}\|^{\boldsymbol{2}}} \cdot \boldsymbol{e_y} = \frac{\|\boldsymbol{\omega} \times \dot{\boldsymbol{\omega}}\|}{\|\boldsymbol{\omega}\|^{\boldsymbol{2}}}, \\
i_4 &= i_4(\boldsymbol{\omega}, \dot{\boldsymbol{\omega}}, \boldsymbol{v}, \dot{\boldsymbol{v}}) = \boldsymbol{e_y} \cdot \dot{\boldsymbol{p}} = \frac{\boldsymbol{\omega} \times \dot{\boldsymbol{\omega}}}{\|\boldsymbol{\omega} \times \dot{\boldsymbol{\omega}}\|} \cdot \frac{(\dot{\boldsymbol{\omega}} \times \boldsymbol{v} + \boldsymbol{\omega} \times \dot{\boldsymbol{v}}) \cdot \|\boldsymbol{\omega}\|^2 - 2(\boldsymbol{\omega} \times \boldsymbol{v}) \cdot (\boldsymbol{\omega} \cdot \dot{\boldsymbol{\omega}})}{\|\boldsymbol{\omega}\|^4}, \\
i_5 &= i_5(\boldsymbol{\omega}, \dot{\boldsymbol{\omega}}, \ddot{\boldsymbol{\omega}}) = \frac{\|(\boldsymbol{\omega} \times \dot{\boldsymbol{\omega}}) \times (\boldsymbol{\omega} \times \ddot{\boldsymbol{\omega}})\|}{\|\boldsymbol{\omega} \times \dot{\boldsymbol{\omega}}\|^2}, \\
i_6 &= i_6(\boldsymbol{\omega}, \dot{\boldsymbol{\omega}}, \ddot{\boldsymbol{\omega}}, \boldsymbol{v}, \dot{\boldsymbol{v}}, \ddot{\boldsymbol{v}}) = \dot{\boldsymbol{p}} \cdot \boldsymbol{e_x} - \dot{p}_2.
\end{aligned}$$

Fig. 3 represents the invariants for one instant of time, $\boldsymbol{\omega_F}$ and $\boldsymbol{v_F}$ are the rotational and the translational velocities of the frame attached to the ISA.

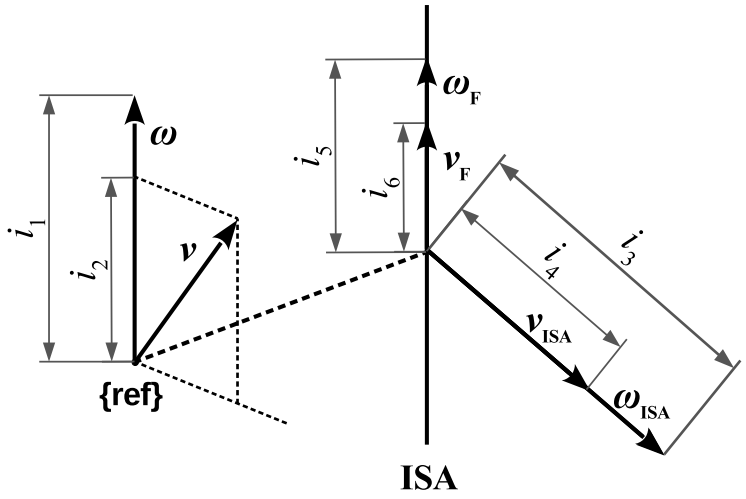

Figure 3.3: Illustrations of Invariants for an instant of time

3.3 Special Cases

3.3.1 Pure Translation

If the rigid body has a certain translation velocity and zero rotational velocity, then the position of the ISA cannot be determined. In this case, the orientation of the ISA is defined to be the same as the orientation of translational velocity. Since the location of the ISA is not defined, the i_4 and i_6 are undetermined. Therefore, the expressions for the invariants are written as follows

$$\begin{aligned} i_1 &= \|\boldsymbol{\omega}\| = 0, \\ i_2 &= \|\boldsymbol{v}\|, \\ i_3 &= \frac{\|\boldsymbol{v} \times \dot{\boldsymbol{v}}\|}{\|\boldsymbol{v}\|^2}, \\ i_4 &- \textit{undetermined}, \\ i_5 &= \frac{\|(\boldsymbol{v} \times \dot{\boldsymbol{v}}) \times (\boldsymbol{v} \times \ddot{\boldsymbol{v}})\|}{\|\boldsymbol{v} \times \dot{\boldsymbol{v}}\|^2}, \\ i_6 &- \textit{undetermined}. \end{aligned} \tag{3.29}$$

3.3.2 Pure Rotation

If the reference point of the rigid body has zero translational velocity, then the expressions for the invariants will take the following form

$$\begin{aligned} i_1 &= \|\boldsymbol{\omega}\|, \\ i_2 &= 0, \\ i_3 &= \frac{\|\boldsymbol{\omega} \times \dot{\boldsymbol{\omega}}\|}{\|\boldsymbol{\omega}\|^{\mathbf{2}}}, \\ i_4 &= 0, \\ i_5 &= \frac{\|(\boldsymbol{\omega} \times \dot{\boldsymbol{\omega}}) \times (\boldsymbol{\omega} \times \ddot{\boldsymbol{\omega}})\|}{\|\boldsymbol{\omega} \times \dot{\boldsymbol{\omega}}\|^2}, \\ i_6 &= 0. \end{aligned} \tag{3.30}$$

3.3.3 ISA with constant orientation: $\dot{\boldsymbol{\omega}} = \mathbf{0}$

In this case, i_5 and i_6 are not defined since the state of the frame attached to the ISA is not uniquely determined. i_4 is also undetermined since the $\boldsymbol{e_y}$ unit vector is not defined. Consequently, the invariants are expressed as

$$\begin{aligned} i_1 &= \|\boldsymbol{\omega}\|, \\ i_2 &= \frac{\boldsymbol{v} \cdot \boldsymbol{\omega}}{\|\boldsymbol{\omega}\|}, \\ i_3 &= 0, \\ i_4 &- undetermined, \\ i_5 &- undetermined, \\ i_6 &- undetermined. \end{aligned} \tag{3.31}$$

3.4 Inverse Problem

In this section, the inverse problem of transition from the invariant description to the traditional description of the rigid body motion will be discussed. The traditional parameters can be written as the functions of the invariants. Depending on the reference point, the velocity vectors can be found from the following equations:

$$\begin{aligned} \boldsymbol{\omega} &= i_1 \cdot \boldsymbol{e_x}, \\ \boldsymbol{v} &= i_2 \cdot \boldsymbol{e_x} + \boldsymbol{p} \times (i_1 \cdot \boldsymbol{e_x}), \end{aligned} \tag{3.32}$$

where $\boldsymbol{p}$ - the vector that starts from the reference point and perpendicular to the ISA. The radius vector and the angular vector would be computed using

$$\begin{aligned}\boldsymbol{r}(t) &= \int_{t_0}^{t} \boldsymbol{v}(t)dt = \int_{t_0}^{t} i_1(t) \cdot \boldsymbol{e_x}(t)dt \\ \boldsymbol{\theta}(t) &= \int_{t_0}^{t} \boldsymbol{\omega}(t)dt = \int_{t_0}^{t} [i_2(t) \cdot \boldsymbol{e_x}(t) + \boldsymbol{p}(t) \times (i_1(t) \cdot \boldsymbol{e_x}(t))]dt. \end{aligned} \tag{3.33}$$

The variables in control functions can be expressed as the functions of the invariants using Eqs. (3.33), and the control function would then be a function of the invariants.

3.5 Motion of Instantaneous Screw Axis

The position of the ISA can be determined by the position of a point from the ISA and the vector $\boldsymbol{e_x}$. With no loss of generality, *central point* $\boldsymbol{o}$ was chosen (see Fig. 3.4), and its motion will be discussed below. If position of the rigid body, Euler angles and velocity vectors are defined as

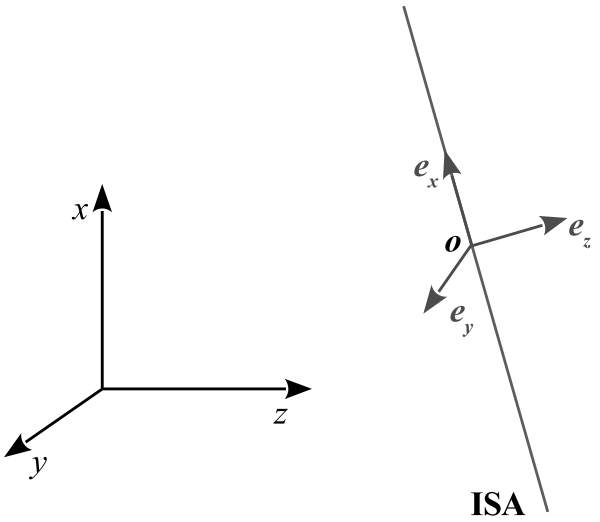

Figure 3.4: ISA in Cartesian coordinate system

$$\boldsymbol{\xi} = \begin{bmatrix} x \\ y \\ z \end{bmatrix}, \boldsymbol{\eta} = \begin{bmatrix} \phi \\ \theta \\ \psi \end{bmatrix}, \dot{\boldsymbol{\xi}} = \boldsymbol{v} = \begin{bmatrix} \dot{x} \\ \dot{y} \\ \dot{z} \end{bmatrix}, \boldsymbol{\omega} = \begin{bmatrix} 1 & 0 & -sin\theta \\ 0 & cos\phi & cos\theta sin\phi \\ 0 & -sin\phi & cos\theta cos\phi \end{bmatrix} \begin{bmatrix} \dot{\phi} \\ \dot{\theta} \\ \dot{\psi} \end{bmatrix}, \tag{3.34}$$

where x, y, z - coordinates of a reference point from the rigid body, then the unit vectors $\boldsymbol{e_x}$ and $\boldsymbol{e_y}$ will be determined as follows:

$$\boldsymbol{e_x} = \frac{\boldsymbol{\omega}}{\|\boldsymbol{\omega}\|} = \begin{bmatrix} (\dot{\phi} - \dot{\psi}sin\theta)/\gamma \\ (\dot{\theta}cos\phi + \dot{\psi}cos\theta sin\phi)/\gamma \\ (\dot{\psi}cos\theta cos\phi - \dot{\theta}sin\phi)/\gamma \end{bmatrix}, \ \boldsymbol{e_y} = \frac{\boldsymbol{\omega} \times \dot{\boldsymbol{\omega}}}{\|\boldsymbol{\omega} \times \dot{\boldsymbol{\omega}}\|}, \tag{3.35}$$

where

$$\gamma = \|\boldsymbol{\omega}\| = \sqrt{\dot{\phi}^2 + \dot{\theta}^2 + \dot{\psi}^2 - 2\dot{\phi}\dot{\psi}sin\theta},$$

$$\dot{\boldsymbol{\omega}} = \begin{bmatrix} \ddot{\phi} - \ddot{\psi}sin\theta - \dot{\psi}\dot{\theta}cos\theta \\ \ddot{\theta}cos\phi - \dot{\theta}\dot{\phi}sin\phi + \ddot{\psi}cos\theta sin\phi - \dot{\psi}\dot{\theta}sin\theta sin\phi + \dot{\phi}\dot{\psi}cos\theta cos\phi \\ \ddot{\psi}cos\theta cos\phi - \dot{\psi}\dot{\theta}sin\theta cos\phi - \dot{\psi}\dot{\phi}cos\theta sin\phi - \ddot{\theta}sin\phi - \dot{\theta}\dot{\phi}cos\phi \end{bmatrix}.$$

The position of the *central point* $\boldsymbol{o}$ can be defined by $\boldsymbol{\zeta}$:

$$\boldsymbol{\zeta} = \begin{bmatrix} \hat{x} & \hat{y} & \hat{z} \end{bmatrix}^T, \tag{3.36}$$

where $\hat{x}, \hat{y}, \hat{z}$ - coordinates of $\boldsymbol{o}$.
The velocity vector of $\boldsymbol{o}$ consists of two component velocities: one is directed along $\boldsymbol{e_x}$ and its value is i_6 (6th invariant), and another is along $\boldsymbol{e_y}$ and its value is i_4 (4th invariant). So, the following expression can be written for the motion of $\boldsymbol{o}$:

$$\dot{\boldsymbol{\zeta}} = i_6 \cdot \boldsymbol{e_x} + i_4 \cdot \boldsymbol{e_y}, \tag{3.37}$$

where

$$i_4 = \boldsymbol{e_y} \cdot \dot{\boldsymbol{p}}, \tag{3.38}$$

$$i_6 = \boldsymbol{e_x} \cdot \dot{\boldsymbol{p}} - \frac{\boldsymbol{d}}{\boldsymbol{dt}} \frac{(\boldsymbol{e_x} \times \boldsymbol{e_y}) \cdot \dot{\boldsymbol{p}} \cdot \|\boldsymbol{\omega}\|^{\boldsymbol{2}}}{\|\boldsymbol{\omega} \times \dot{\boldsymbol{\omega}}\|}. \tag{3.39}$$

Eq. (3.37) is the equation of motion of the *central point* $\boldsymbol{o}$. Eq. (3.35) and Eq. (3.37) are adequate to define the motion of the ISA. Now, the expressions of i_4 and i_6 as the functions of the control parameters are discussed below. According to Newton's second law

$$\begin{aligned} m\ddot{\boldsymbol{r}} &= \boldsymbol{F}, \\ \boldsymbol{I}\ddot{\boldsymbol{\theta}} &= \boldsymbol{\tau}, \end{aligned} \tag{3.40}$$

where $\boldsymbol{F}$ is the total force, $\boldsymbol{\tau}$ is the total torque, m is the mass of the rigid body, $\boldsymbol{I}$ is the inertia matrix. It is known that

$$\boldsymbol{F} = \frac{d\boldsymbol{P}}{dt},\ \boldsymbol{\tau} = \frac{d\boldsymbol{L}}{dt}, \tag{3.41}$$

where $\boldsymbol{P}$ and $\boldsymbol{L}$ are the linear and angular momentums respectively. Eq. (3.38) and (3.39) become as

$$i_4 = \boldsymbol{e_y} \cdot \dot{\boldsymbol{p}} = \frac{(\hat{\boldsymbol{L}} \times \hat{\boldsymbol{\tau}})}{\|\hat{\boldsymbol{L}} \times \hat{\boldsymbol{\tau}}\|} \cdot \frac{(\hat{\boldsymbol{\tau}} \times \boldsymbol{P} + \hat{\boldsymbol{L}} \times \boldsymbol{F})\|\hat{\boldsymbol{L}}\|^2 - 2(\hat{\boldsymbol{L}} \times \boldsymbol{P}) \cdot (\hat{\boldsymbol{L}} \cdot \hat{\boldsymbol{\tau}})}{m\|\hat{\boldsymbol{L}}\|^4}, \tag{3.42}$$

$$\begin{aligned} i_6 =& \frac{\hat{\boldsymbol{L}} \cdot (\hat{\boldsymbol{\tau}} \times \boldsymbol{P})}{m\|\hat{\boldsymbol{L}}\|^2} - \\ & - \frac{d}{dt}\left[\frac{(\hat{\boldsymbol{L}} \times (\hat{\boldsymbol{L}} \times \hat{\boldsymbol{\tau}}))}{\|\hat{\boldsymbol{L}} \times \hat{\boldsymbol{\tau}}\|^2} \cdot \frac{(\hat{\boldsymbol{\tau}} \times \boldsymbol{P} + \hat{\boldsymbol{L}} \times \boldsymbol{F})\|\hat{\boldsymbol{L}}\|^2 - 2(\hat{\boldsymbol{L}} \times \boldsymbol{P}) \cdot (\hat{\boldsymbol{L}} \cdot \hat{\boldsymbol{\tau}})}{m\|\hat{\boldsymbol{L}}\|^3}\right], \end{aligned} \tag{3.43}$$

where $\hat{\boldsymbol{L}} = \boldsymbol{I^{-1}L}, \hat{\boldsymbol{\tau}} = \boldsymbol{I^{-1}\tau}$. If the rigid body is a quadcopter, then the inertia matrix can be written as

$$\boldsymbol{I} = \begin{bmatrix} I_x & 0 & 0 \\ 0 & I_y & 0 \\ 0 & 0 & I_z \end{bmatrix}. \tag{3.44}$$

And, Eqs. (3.42) and (3.43) can be written in scalar forms. The scalar expressions for i_4 and i_6 are shown in Appendix B.

CHAPTER 4
ISM INVARIANTS IN QUADCOPTER MOTION

4.1 Control Problem in Quadcopter

The dynamic model of the quadcopter shows that the angular rates of the four rotors can be considered as the control parameters, and they can be found from the Eqs. (2.6) and (2.11) as

$$\begin{aligned}
\omega_1^2 &= \frac{T}{4k} - \frac{\tau_\theta}{2kl} - \frac{\tau_\psi}{4b}, \\
\omega_2^2 &= \frac{T}{4k} - \frac{\tau_\phi}{2kl} + \frac{\tau_\psi}{4b}, \\
\omega_3^2 &= \frac{T}{4k} + \frac{\tau_\theta}{2kl} - \frac{\tau_\psi}{4b}, \\
\omega_4^2 &= \frac{T}{4k} + \frac{\tau_\phi}{2kl} + \frac{\tau_\psi}{4b},
\end{aligned} \tag{4.1}$$

where $\tau_\phi,\ \tau_\theta,\ \tau_\psi$ - torque components, k - lift constant, b_τ - torque drag coefficient.
The quadcopter has six degrees of freedom and only four control parameters. Eqs. (4.1) show that the control parameters can be found by calculating the thrust and torque. In most cases, linear controllers such as the PID controller, are used to control the UAVs. Due to its simplicity, the PD controller was chosen to control the quadcopter.

4.2 PD controller

The mathematical representation of the PD controller is given by the following equation:

$$\begin{aligned}
e(t) &= s_d(t) - s(t), \\
u(t) &= K_P e(t) + K_D \frac{de(t)}{dt},
\end{aligned} \tag{4.2}$$

where $s_d(t)$ - desired state, $s(t)$ - current state, $e(t)$ - difference between the desired state and the current state, $u(t)$ - control input, $K_P,\ K_D$ - proportional and derivative control gains respectively [47].
The state vector in the quadcopter dynamics is given as

$$\boldsymbol{s} = [\boldsymbol{\xi} \quad \boldsymbol{v} \quad \boldsymbol{\eta} \quad \boldsymbol{\omega}], \tag{4.3}$$

where $\boldsymbol{\xi},\ \boldsymbol{\eta}$ - linear and angular position vectors, $\boldsymbol{v},\ \boldsymbol{\omega}$ - linear and angular velocity vectors respectively.

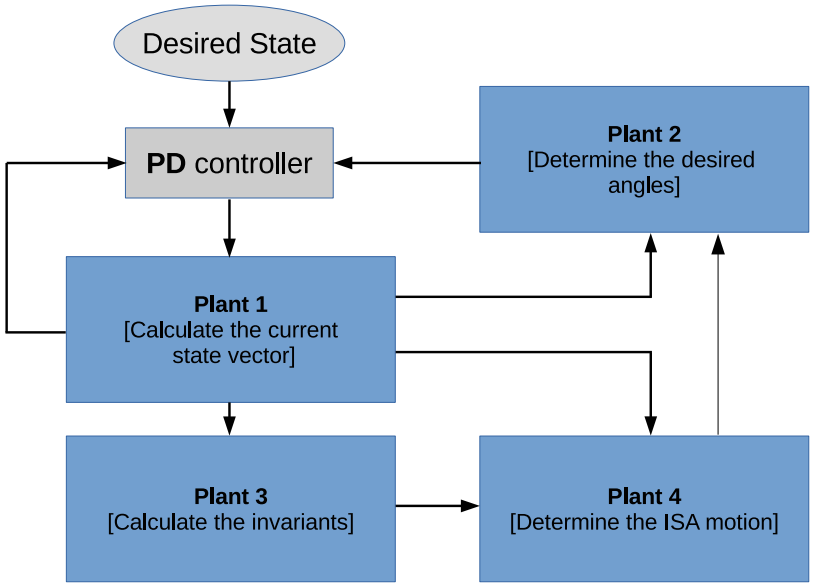

Figure 4.1: Quadcopter Control Algorithm

In order to calculate the thrust and torque, the PD controller can be utilized in the following form:

$$\begin{aligned} T &= \left[K_P^z(z_d - z) + K_D^z(\dot{z}_d - \dot{z}) + g\right] \frac{m}{cos\phi cos\theta}, \\ \tau_\phi &= \left[K_P^\phi(\phi_d - \phi) + K_D^\phi(\dot{\phi}_d - \dot{\phi})\right] I_{xx}, \\ \tau_\theta &= \left[K_P^\theta(\theta_d - \theta) + K_D^\theta(\dot{\theta}_d - \dot{\theta})\right] I_{yy}, \\ \tau_\psi &= \left[K_P^\psi(\psi_d - \psi) + K_D^\psi(\dot{\psi}_d - \dot{\psi})\right] I_{zz}, \end{aligned} \tag{4.4}$$

where g - gravitational acceleration, m - mass, $\phi,\ \theta,\ \psi$ - Euler angles (subscript d indicates "desired"), $I_{xx},\ I_{yy},\ I_{zz}$ - inertia matrix components [48].
In this case, the x and y positions of the quadcopter are not controlled. To control them as well, the algorithm that is shown in Figure 4.1 can be developed. In Plant 2, the desired angles are determined from the current thrust vector and the linear position error vector ($\boldsymbol{\xi_d} - \boldsymbol{\xi}$).
To implement the simulation, the values for the parameters have been chosen similar to the values given in [49], and are shown in Table 4.1. The PD controller parameters are given in Table 4.2.

4.3 Other Controllers in Invariant Calculations

Other controllers can also be used to calculate the invariants. However, depending on the structure of the controller it can create a difficulty and additional errors in calculations. For example, let's

Parameter	Value	Unit
m	0.47	kg
g	9.81	m/s^2
l	0.225	m
b_τ	$1.15 \cdot 10^{-7}$	
k	$3 \cdot 10^{-6}$	

Parameter	Value	Unit
I_{xx}	$4.86 \cdot 10^{-3}$	$kg \cdot m^2$
I_{yy}	$4.86 \cdot 10^{-3}$	$kg \cdot m^2$
I_{zz}	$8.80 \cdot 10^{-3}$	$kg \cdot m^2$
k_d	0.25	kg/s

Table 4.1: Parameter values

Parameter	Value
K_P^x	0.5
K_P^y	0.5
K_P^z	1.5
K_P^ϕ	6
K_P^θ	6
K_P^ψ	6

Parameter	Value
K_D^x	0.5
K_D^y	0.5
K_D^z	2.5
K_D^ϕ	1.75
K_D^θ	1.75
K_D^ψ	1.75

Table 4.2: Parameters for the PD controller.

consider the PID controller. The mathematical expression of the PID controller is given as

$$\begin{aligned} e(t) &= s_d(t) - s(t), \\ u(t) &= K_P e(t) + K_I \int_0^t e(\tau) d\tau + K_D \frac{de(t)}{dt}, \end{aligned} \tag{4.5}$$

where K_I - integral gain.

The difference between the expressions for the PID and PD controllers is the integral term in the PID controller, which requires integrating the error. In numerical integration of the equations of motion, this term adds one more step of integration which can increase the systematic error in determining the state vector components in this example. In this example, the current state vector is calculated from the controller outputs (i.e thrust and torque). However, during the real flight of the quadcopter, the current state vector components are determined from the sensors, and the integration term wouldn't really have an effect on the accuracy of the current state vector as well as the invariants.

Studying the PID controller using the invariants and fractional derivatives is one of the future works.

4.4 Alternative Control Laws

Using the linear controllers in nonlinear systems can create a systematic error. These types of errors can be reduced by either linearizing the nonlinear dynamical system properly or developing

nonlinear controllers.

Linearization of a nonlinear system can be implemented using linearization and approximation methods. These methods can include Lyapunov methods, analytical linearization, forward, backward, and centered approximation methods, etc. [50], [51].

Nonlinear controllers can also be developed using analytical linearization and approximation methods. In most cases, the nonlinear controllers change depending on the nonlinear dynamical system. There are a lot of works devoted to the nonlinear control problem. For example, A. Matus-Vargas et al. used gradient optimization strategies and Pontryagin's maximum principle to control nonlinear UAV models [39]. In another work, a nonlinear super-twisting controller was developed based on Lyapunov methods to stabilize the quadcopter's attitude [52].

4.5 Profiles of ISM Parameters

In this section, instantaneous screw motion (ISM) parameters will be calculated for particular cases of the quadcopter's motion. The goal is to see how each invariant changes depending on the state vector. First of all, two similar maneuvers will be tested, and the profiles of the invariants and the instantaneous screw axis (ISA) obtained for both cases will be contrasted.

4.5.1 Example A: Transfer of Quadcopter

This example considers the transfer of the quadcopter between two given configurations:

Example 1
Initial state: $\boldsymbol{\xi}_0 = [0\ 0\ 2]$, $\boldsymbol{\eta}_0 = [0.2\ 0.2\ 0.2]$;
Desired state: $\boldsymbol{\xi}_d = [0\ 0\ 0]$, $\boldsymbol{\eta}_d = [0\ 0\ 0]$;
with zero initial and final velocities.

Profiles of State vector
Utilizing the PD controller described in the previous section, the simulation results shown in Figure 4.2 can be obtained for the state vector. Figure 4.2 shows the coordinates of the center of mass of the quadcopter (a), Euler angles (b), translational velocity (c), and rotational velocity (d).

Profiles of Invariants
The profiles of the invariants for this particular motion are presented in Figure 4.3. The units of $i_{1,3,5}$ are rad/sec since they are defining the rotational velocities. The units of $i_{2,4,6}$ are m/sec as they are defining the translational velocities. Since the $\boldsymbol{e_x}$ unit vector has been chosen in the same direction with the rotational velocity vector, the values of i_1, i_3, i_5 become always positive.

Profiles of ISA
In Figure 4.4, the position of central point and the direction of $\boldsymbol{e_x}$ unit vector are presented.

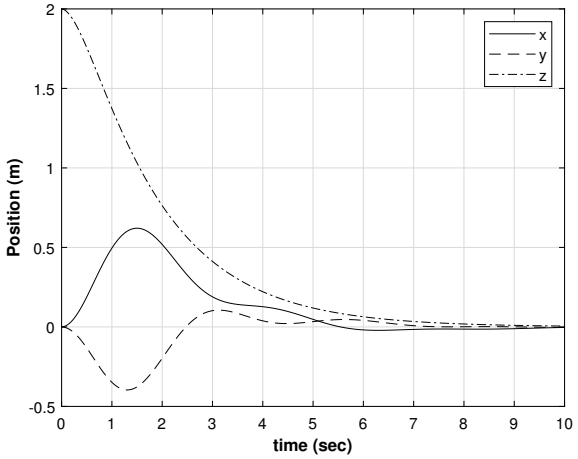

(a) Position

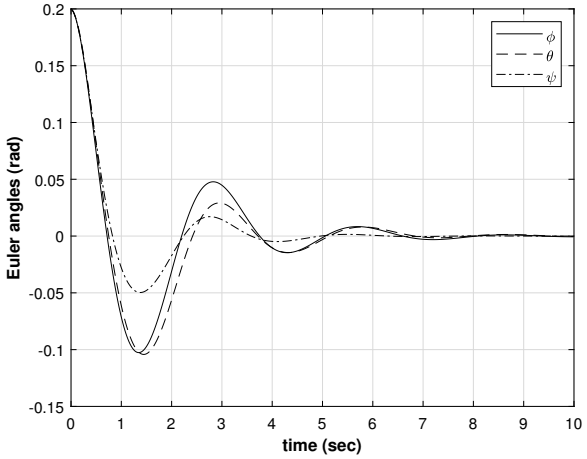

(b) Euler angles

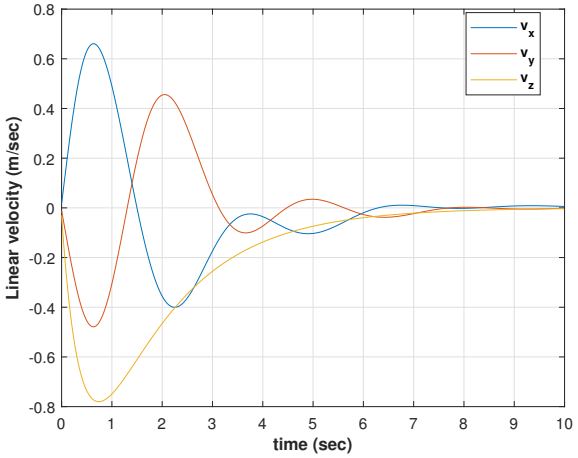

(c) Linear velocity

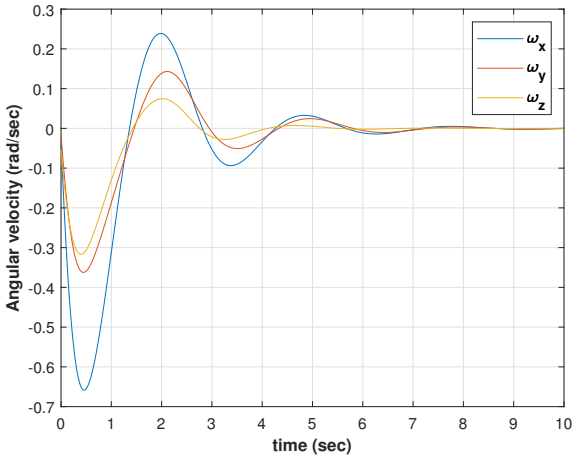

(d) Angular velocity

Figure 4.2: State vector components

Example 2

Initial state: $\boldsymbol{\xi}_0 = [0\ 0\ 0]$, $\boldsymbol{\eta}_0 = [0.2\ 0.2\ 0.2]$;
Desired state: $\boldsymbol{\xi}_d = [2\ 3\ 10]$, $\boldsymbol{\eta}_d = [0\ 0\ 0]$;
with zero initial and final velocities.

Profiles of State vector

The profiles of the state vector components are given in Figure 4.5.

Profiles of Invariants

Figure 4.6 shows the profiles of the invariants for this example.

Profiles of ISA

Figure 4.7 shows the trajectory of the central point $\boldsymbol{o}$ (a), the direction of $\boldsymbol{e_x}$ (b), and their combination. By combining Figure 4.7a and 4.7b, we can create the state of the ISA, which is represented in Figure 4.7c. To make this graph clearer, the number of $\boldsymbol{e_x}$ has been reduced: there are some points without $\boldsymbol{e_x}$. In Figure 4.7d, the ISA's initial and final state are represented. Figure 4.7e shows the ISA and the quadcopter frame at three consecutive moments.

One can see from the figures that the invariants have similar patterns in both examples. In addition, their profiles indicate that they might have a certain period in which they repeat the same (or proportional) values. One reason for the similar profiles of the invariants might be the similarity in the maneuvers (in both cases the initial and final velocities are zero). In the next example, a more general motion of the quadcopter will be studied.

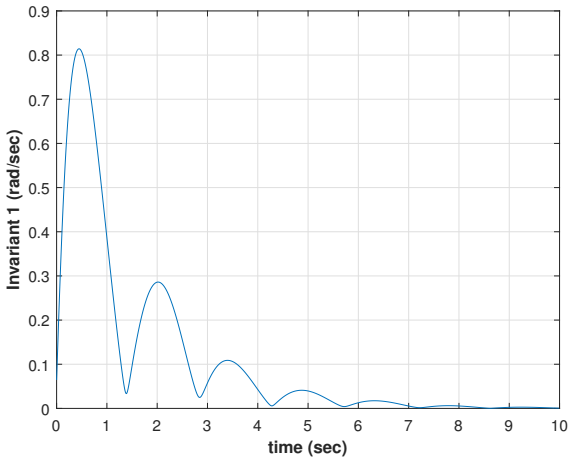

(a)

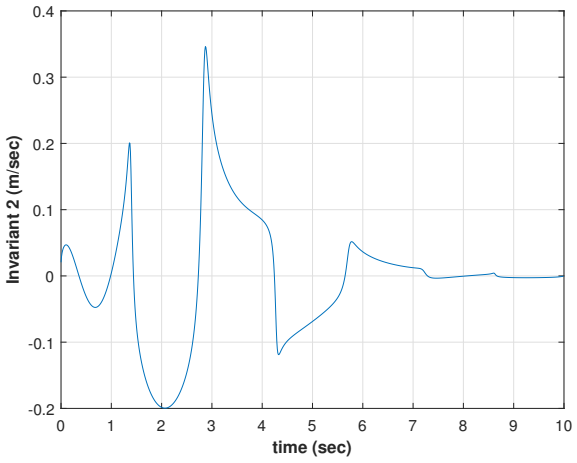

(b)

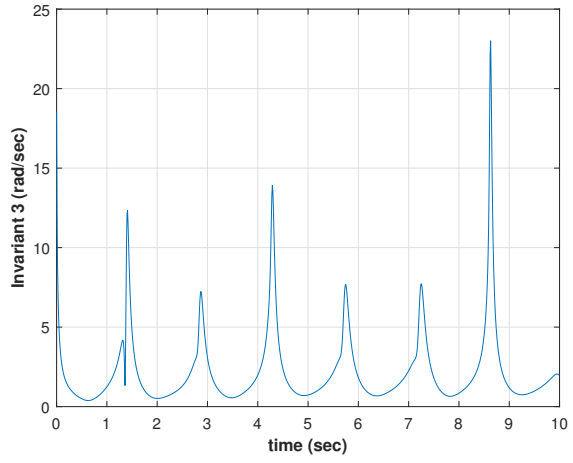

(c)

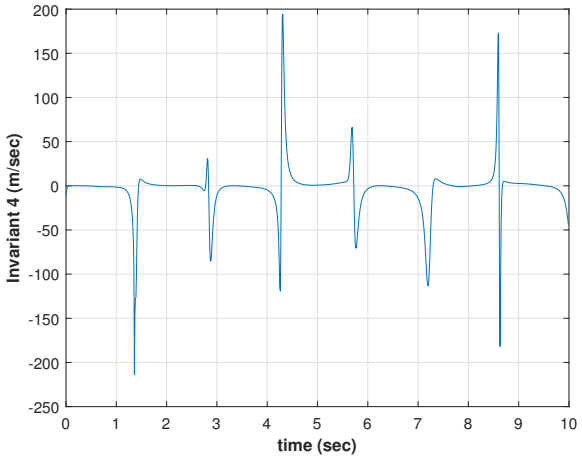

(d)

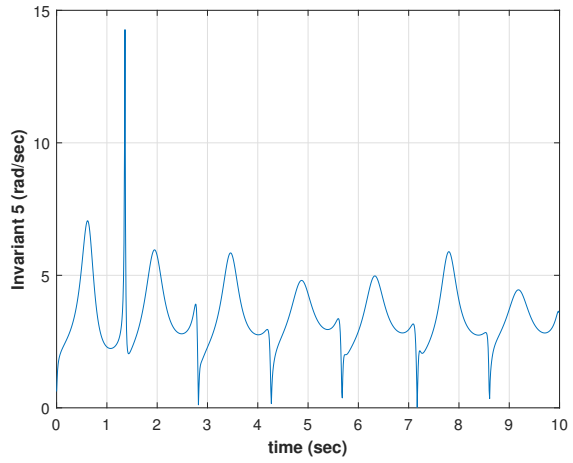

(e)

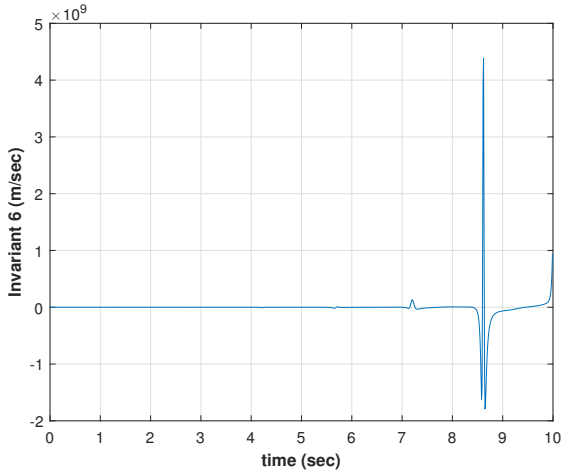

(f)

Figure 4.3: Profiles of Invariants

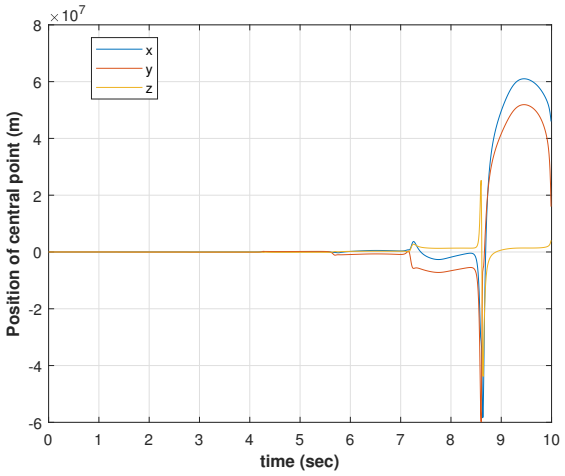

(a) Position of central point in 2D

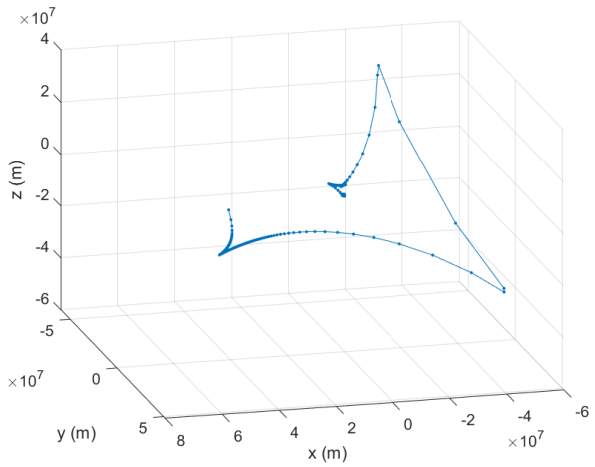

(b) Position of central point in 3D

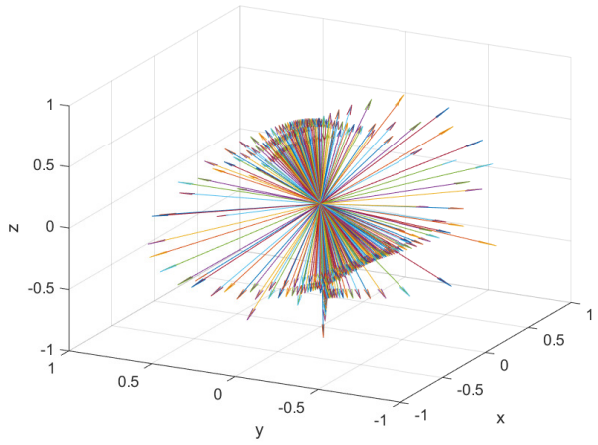

(c) Direction of $\boldsymbol{e_x}$

Figure 4.4: Profile of ISA

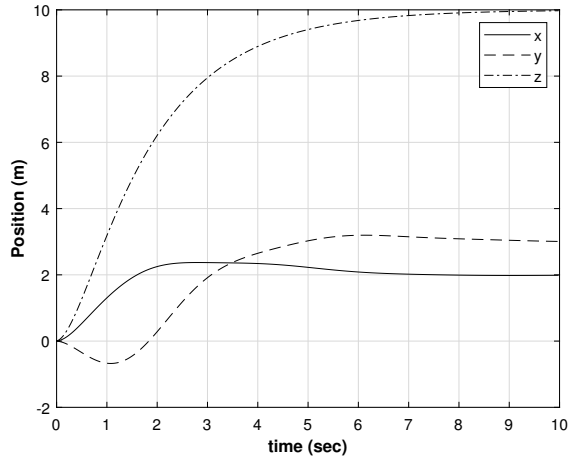

(a) Position of quadcopter

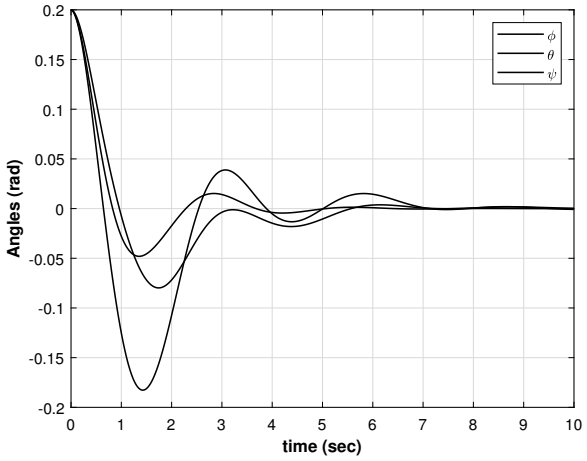

(b) Euler angles

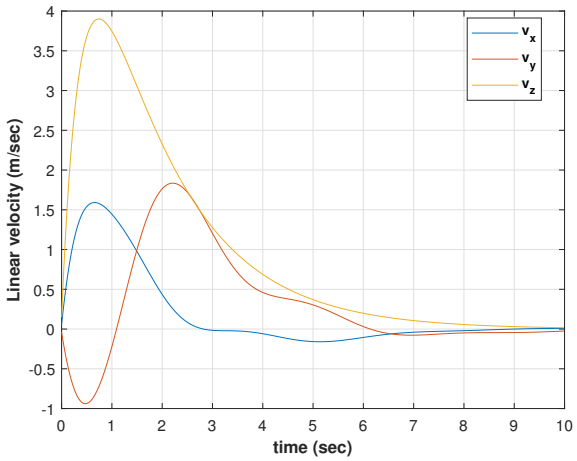

(c) Linear velocity

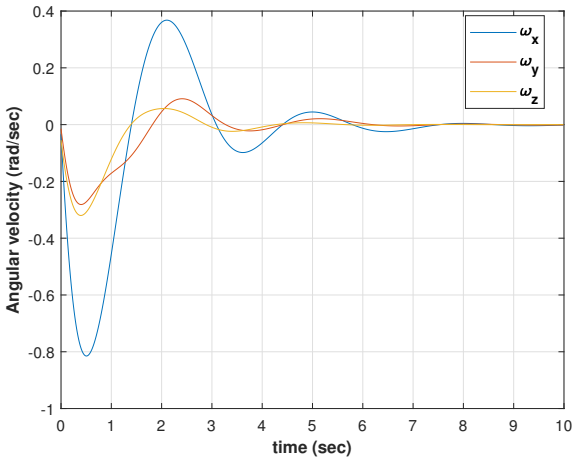

(d) Angular velocity

Figure 4.5: State vector

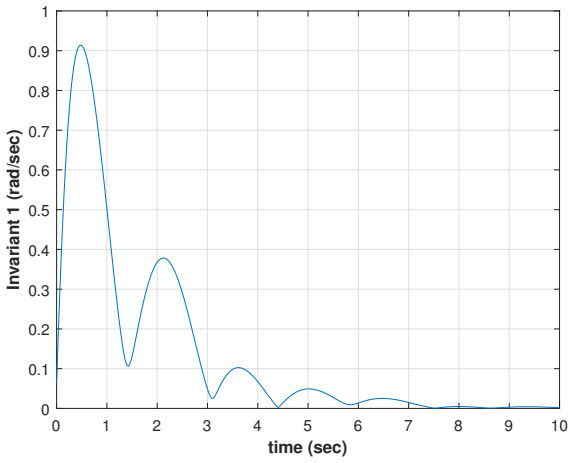

(a)

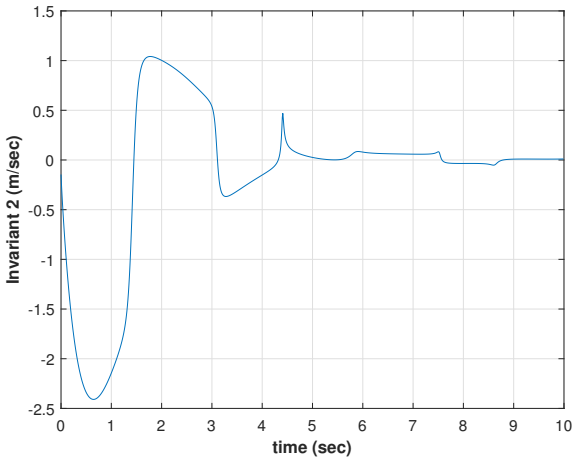

(b)

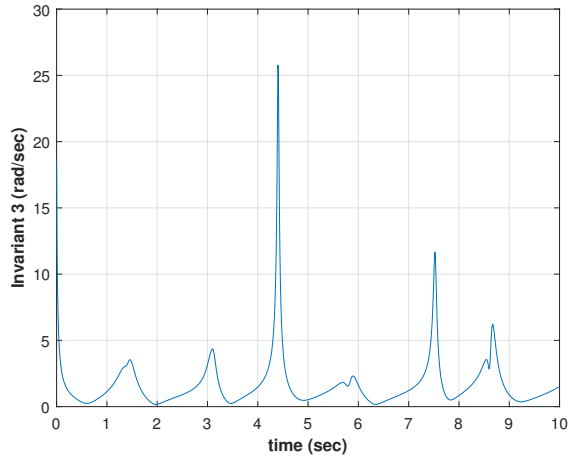

(c)

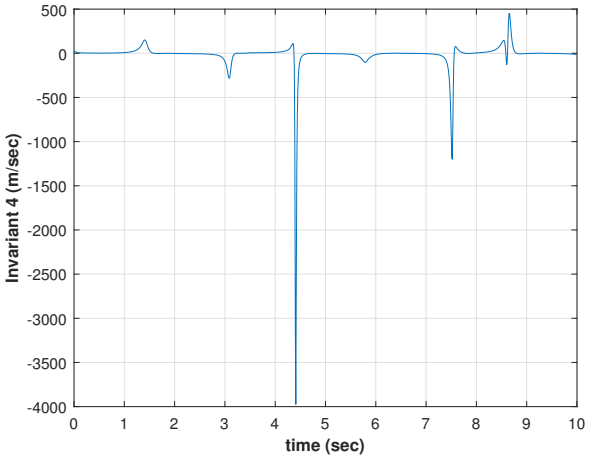

(d)

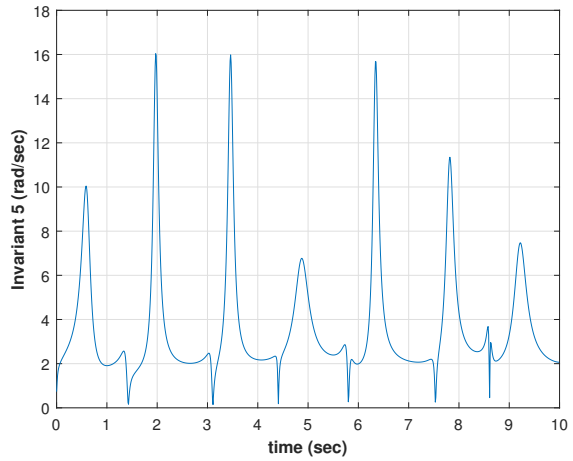

(e)

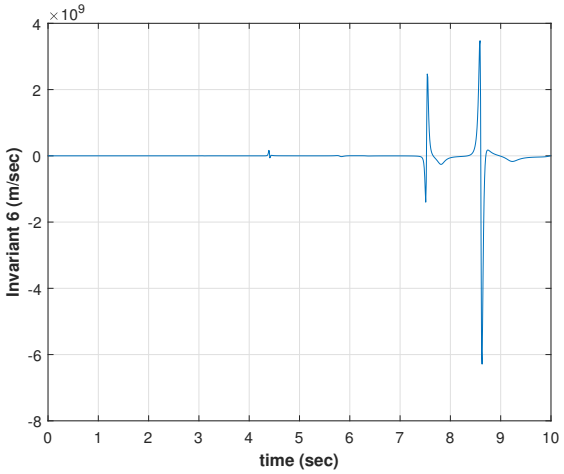

(f)

Figure 4.6: Profiles of Invariants

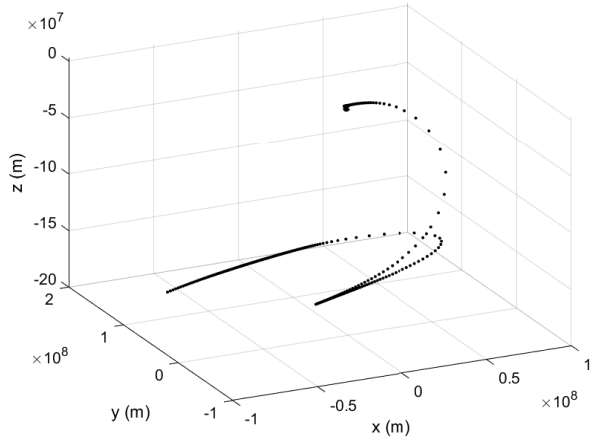

(a) Position of the central point ($\boldsymbol{o}$)

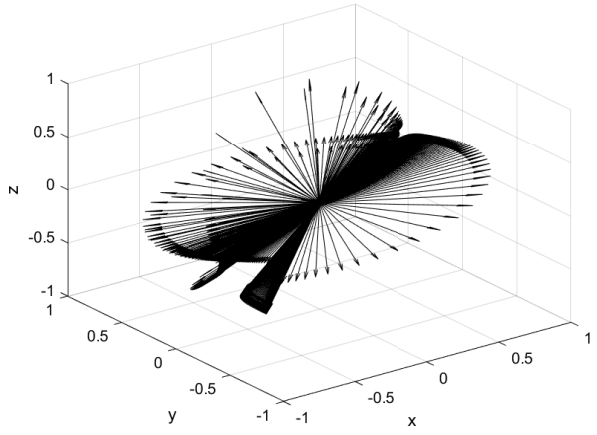

(b) Direction of $\boldsymbol{e_x}$

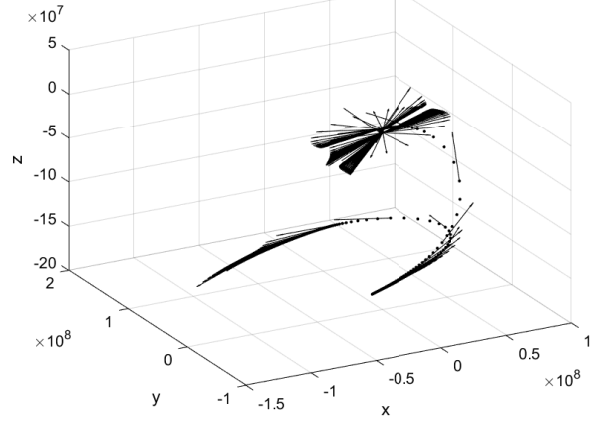

(c) State of the ISA

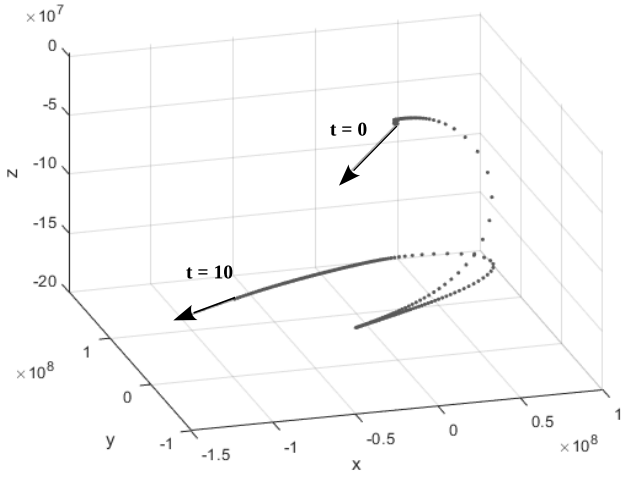

(d) ISA at t=0 and t=10

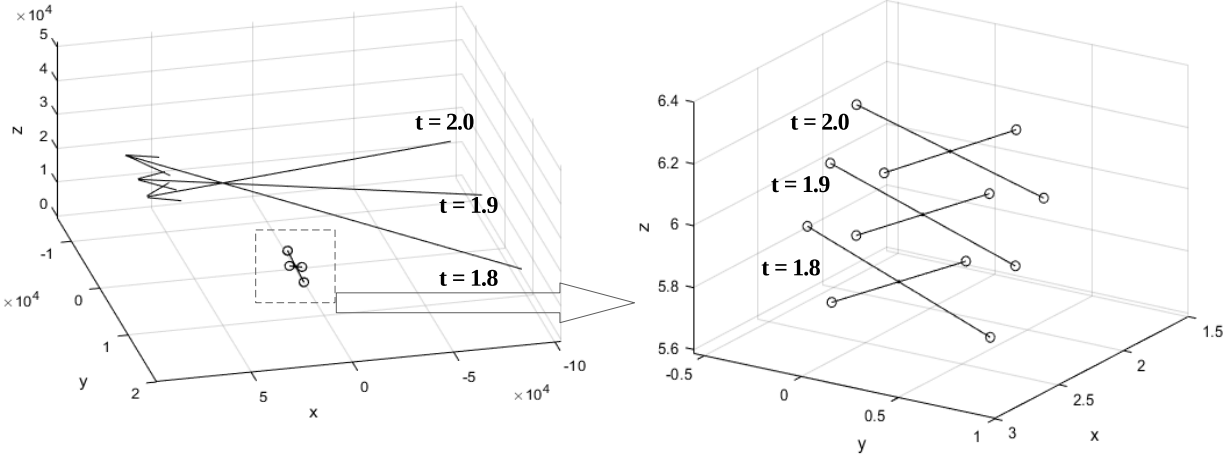

(e) ISA at three consecutive time instants

Figure 4.7: Profiles of the ISA

4.5.2 Example B: Trajectory Follow

Now, another example of the quadcopter's motion will considered. In this example, the quadcopter has to take the photos of the network of water tubes shown in Figure 4.8. The dash-dot (-.-.-) line is the trajectory that the quadcopter should follow. In this case, the coordinates of the points are as follows:

$\boldsymbol{A}$(0 20 0), $\boldsymbol{B}$(20 20 0), $\boldsymbol{C}$(20 35 0), $\boldsymbol{D}$(0 35 10), $\boldsymbol{E}$(0 65 0).

The quadcopter, firstly, takes off the ground 10 meters, and then starts following the trajectory taking photos of the tubes. After reaching the end of the tube, the quadcopter comes back at the hight of 12 meters, and then, lands. The continues line in Figure 4.9e is the path that the

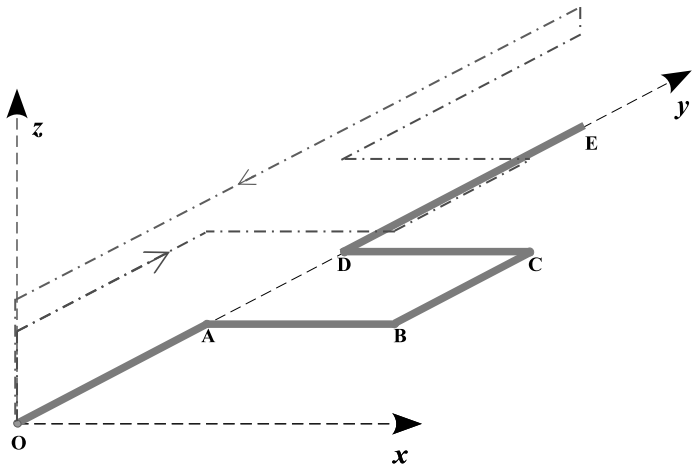

Figure 4.8: Network of tubes

quadcopter should follow, while the dashed line is the actual trajectory of the quadcopter. The motion lasts about 43 seconds.

Figure 4.9 represents the position of the quadcopter (a), Euler angles (b), the coordinates of the central point $\boldsymbol{o}$ (c), and the direction of $\boldsymbol{e_x}$ (d).

In Figure 4.10 , one can see that Invariant 4 and Invariant 6 are unknown for a while at the beginning of the motion. This is because of the special case where the angular velocity $\boldsymbol{\omega}$ is equal to zero.

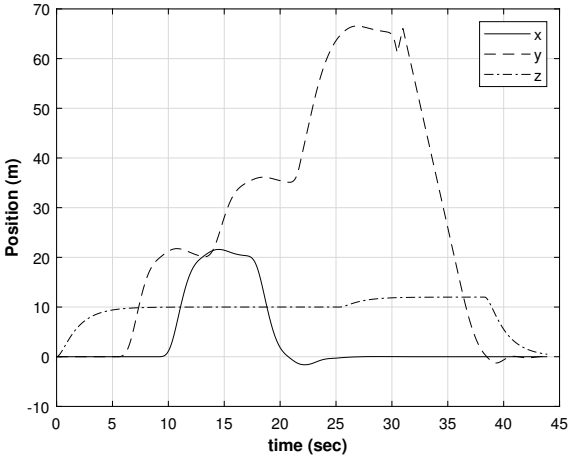

(a) The position of the quadcopter

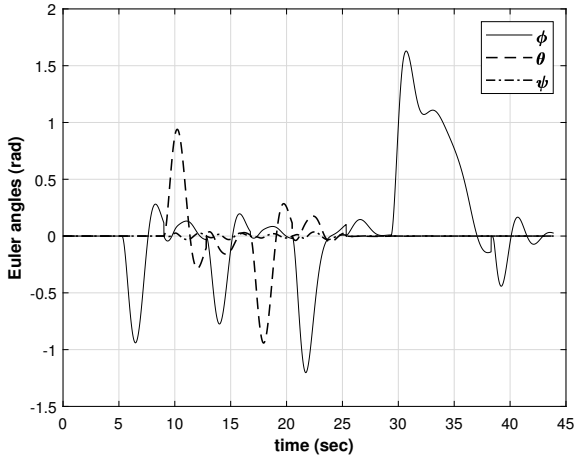

(b) Euler angles

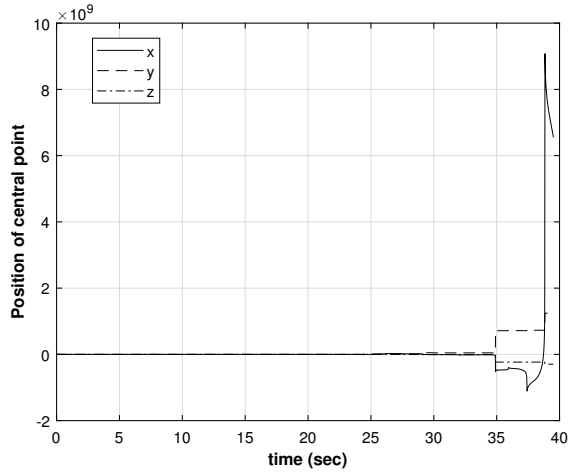

(c) The position of the central point

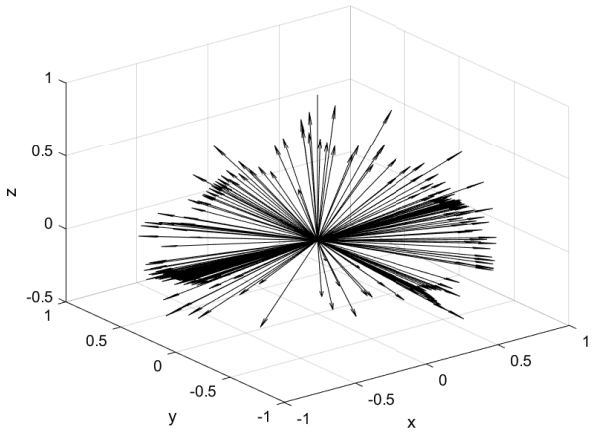

(d) The change of the direction of $\boldsymbol{e_x}$

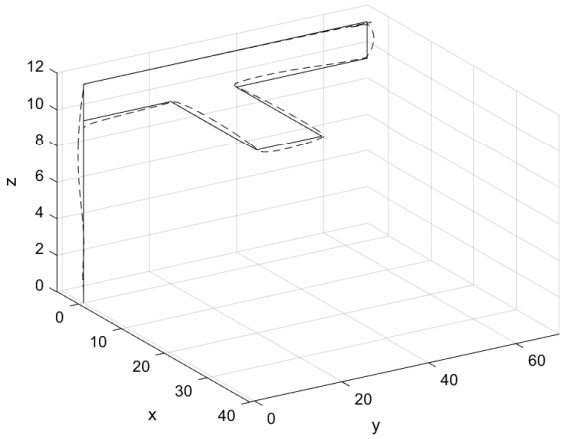

(e) Trajectory of Quadcopter

Figure 4.9: Simulation results

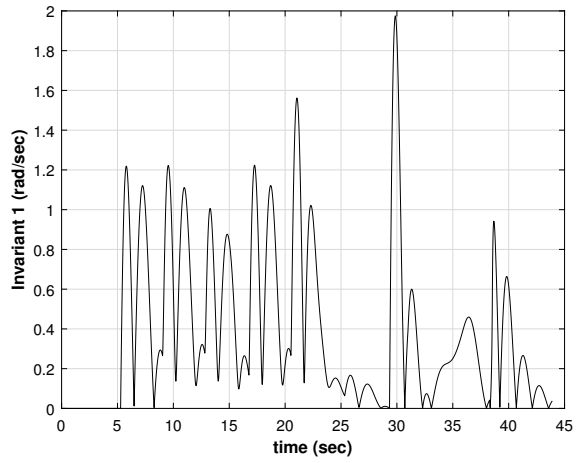

(a)

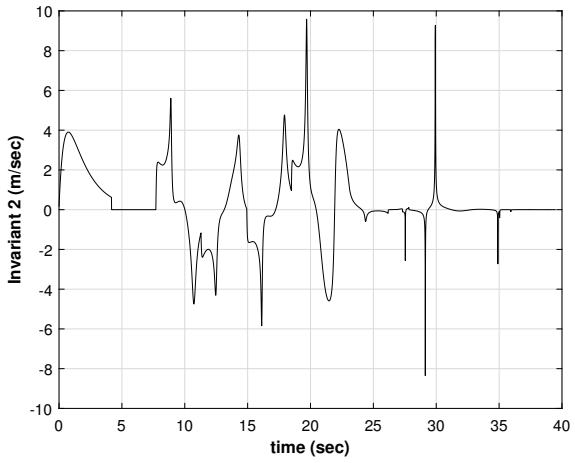

(b)

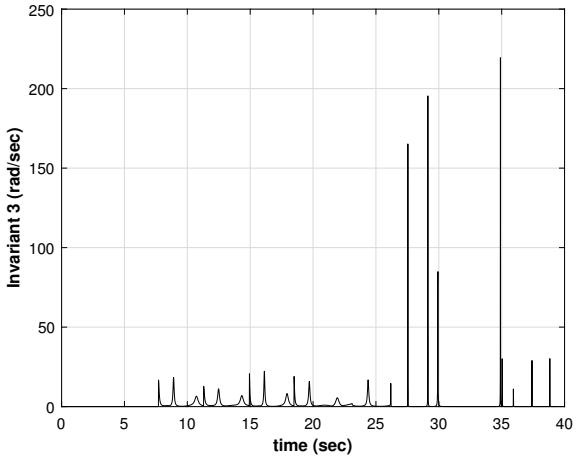

(c)

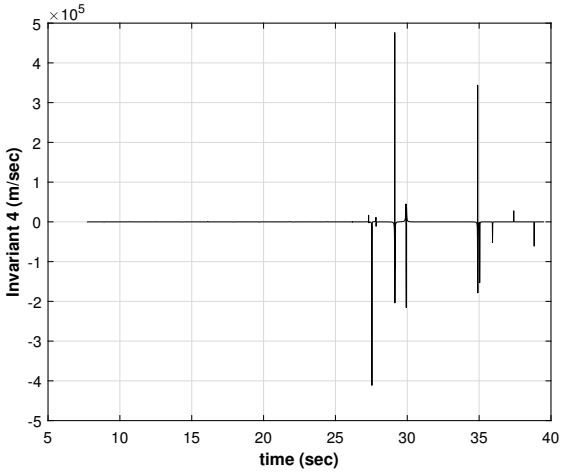

(d)

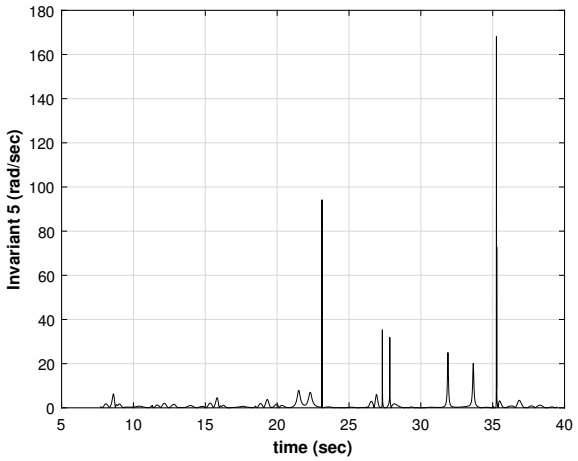

(e)

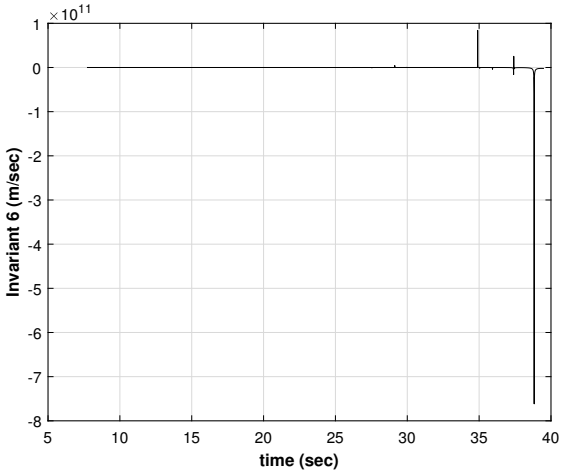

(f)

Figure 4.10: Invariants

CHAPTER 5
ISM INVARIANTS IN FIXED-WING UAV MOTION

5.1 Expressions of Invariants

The dynamic model of a fixed-wing unmanned aerial vehicle (UAV) has been represented in Section 2.2 where the aircraft was assumed to be in motion on a vertical plane. The following main assumptions were made to obtain the particular equations of motion and the expressions for the control parameters: a) bank angle is constant, b) sideslip angle is zero, and c) mass is constant. The general form of the expressions for six invariants i_k, $(k = 1, ..., 6)$ are given as follows :

$$\begin{aligned} i_1 &= f_1(\boldsymbol{\omega}), \\ i_2 &= f_2(\boldsymbol{\omega}, \boldsymbol{v}), \\ i_3 &= f_3(\boldsymbol{\omega}, \dot{\boldsymbol{\omega}}), \\ i_4 &= f_4(\boldsymbol{\omega}, \dot{\boldsymbol{\omega}}, \boldsymbol{v}, \dot{\boldsymbol{v}}), \\ i_5 &= f_5(\boldsymbol{\omega}, \dot{\boldsymbol{\omega}}, \ddot{\boldsymbol{\omega}}), \\ i_6 &= f_6(\boldsymbol{\omega}, \dot{\boldsymbol{\omega}}, \ddot{\boldsymbol{\omega}}, \boldsymbol{v}, \dot{\boldsymbol{v}}, \ddot{\boldsymbol{v}}), \end{aligned} \tag{5.1}$$

where $\boldsymbol{\omega}$ and $\boldsymbol{v}$ are the angular and translational velocity vectors respectively [2, 53].
If the bank angle is constant (assumption a), then the angular velocity vector can be derived in the following form:

$$\boldsymbol{\omega} = \frac{\dot{\boldsymbol{r}} \times \ddot{\boldsymbol{r}}}{\|\dot{\boldsymbol{r}}\|^2}, \tag{5.2}$$

where $\boldsymbol{r}$ is the linear position vector of the aircraft [31].
The linear velocity can be written in terms of $\boldsymbol{r}$ as

$$\boldsymbol{v} = \dot{\boldsymbol{r}}. \tag{5.3}$$

Substitution of Eqs. 5.2 and 5.3 into the expressions for the invariants yields

$$
\begin{aligned}
i_1 &= \|\boldsymbol{\omega}\| = \frac{\|\dot{\boldsymbol{r}} \times \ddot{\boldsymbol{r}}\|}{\|\dot{\boldsymbol{r}}\|^2}, \\
i_2 &= \frac{\boldsymbol{v} \cdot \boldsymbol{\omega}}{\|\boldsymbol{\omega}\|} = 0, \\
i_3 &= \frac{\|\boldsymbol{\omega} \times \dot{\boldsymbol{\omega}}\|}{\|\boldsymbol{\omega}\|^2} = \frac{\|(\dot{\boldsymbol{r}} \times \ddot{\boldsymbol{r}}) \times (\dot{\boldsymbol{r}} \times \dddot{\boldsymbol{r}})\|}{\|\dot{\boldsymbol{r}}\|^2 \|\dot{\boldsymbol{r}} \times \ddot{\boldsymbol{r}}\|}, \\
i_4 &= \frac{(\dot{\boldsymbol{r}} \times \ddot{\boldsymbol{r}}) \times (\dot{\boldsymbol{r}} \times \dddot{\boldsymbol{r}})}{\|(\dot{\boldsymbol{r}} \times \ddot{\boldsymbol{r}}) \times (\dot{\boldsymbol{r}} \times \dddot{\boldsymbol{r}})\|} \\
&\quad \cdot \left[\frac{(\dot{\boldsymbol{r}} \times \dddot{\boldsymbol{r}}) \times \dot{\boldsymbol{r}} + (\dot{\boldsymbol{r}} \times \ddot{\boldsymbol{r}}) \times \ddot{\boldsymbol{r}}}{\|\dot{\boldsymbol{r}} \times \ddot{\boldsymbol{r}}\|} - \frac{2\|\dot{\boldsymbol{r}}\|^4 \{(\dot{\boldsymbol{r}} \times \ddot{\boldsymbol{r}}) \times (\dot{\boldsymbol{r}} \times \dddot{\boldsymbol{r}})\} \cdot \{(\dot{\boldsymbol{r}} \times \ddot{\boldsymbol{r}}) \times \dot{\boldsymbol{r}}\}}{\|\dot{\boldsymbol{r}} \times \ddot{\boldsymbol{r}}\|^4} \right], \\
i_5 &= \frac{\|[(\dot{\boldsymbol{r}} \times \ddot{\boldsymbol{r}}) \times (\dot{\boldsymbol{r}} \times \dddot{\boldsymbol{r}})] \times [(\dot{\boldsymbol{r}} \times \ddot{\boldsymbol{r}}) \times (\dot{\boldsymbol{r}} \times \dddot{\boldsymbol{r}} + \dot{\boldsymbol{r}} \times \overset{(4)}{\boldsymbol{r}})]\|}{\|\dot{\boldsymbol{r}}\|^4 \|(\dot{\boldsymbol{r}} \times \ddot{\boldsymbol{r}}) \times (\dot{\boldsymbol{r}} \times \dddot{\boldsymbol{r}})\|}, \\
i_6 &= \dot{\boldsymbol{p}} \cdot \boldsymbol{e}_x - \dot{p}_2,
\end{aligned}
\tag{5.4}
$$

where

$$
\begin{aligned}
\dot{\boldsymbol{p}} &= \frac{(\dot{\boldsymbol{r}} \times \dddot{\boldsymbol{r}}) \times \dot{\boldsymbol{r}} + (\dot{\boldsymbol{r}} \times \ddot{\boldsymbol{r}}) \times \ddot{\boldsymbol{r}}}{\|\dot{\boldsymbol{r}} \times \ddot{\boldsymbol{r}}\|} - \frac{2\|\dot{\boldsymbol{r}}\|^4 \{(\dot{\boldsymbol{r}} \times \ddot{\boldsymbol{r}}) \times (\dot{\boldsymbol{r}} \times \dddot{\boldsymbol{r}})\} \cdot \{(\dot{\boldsymbol{r}} \times \ddot{\boldsymbol{r}}) \times \dot{\boldsymbol{r}}\}}{\|\dot{\boldsymbol{r}} \times \ddot{\boldsymbol{r}}\|^4}, \\
\boldsymbol{e}_x &= \frac{\dot{\boldsymbol{r}} \times \ddot{\boldsymbol{r}}}{\|\dot{\boldsymbol{r}} \times \ddot{\boldsymbol{r}}\|}, \quad \boldsymbol{e}_z = \frac{[\dot{\boldsymbol{r}} \times \ddot{\boldsymbol{r}}] \times [(\dot{\boldsymbol{r}} \times \ddot{\boldsymbol{r}}) \times (\dot{\boldsymbol{r}} \times \dddot{\boldsymbol{r}})]}{\|\dot{\boldsymbol{r}} \times \ddot{\boldsymbol{r}}\| \cdot \|(\dot{\boldsymbol{r}} \times \ddot{\boldsymbol{r}}) \times (\dot{\boldsymbol{r}} \times \dddot{\boldsymbol{r}})\|}, \\
p_2 &= -\frac{\boldsymbol{p} \cdot \boldsymbol{e}_z}{\omega_2}, \quad \omega_2 = \frac{\|(\dot{\boldsymbol{r}} \times \ddot{\boldsymbol{r}}) \times (\dot{\boldsymbol{r}} \times \dddot{\boldsymbol{r}})\|}{\|\dot{\boldsymbol{r}} \times \ddot{\boldsymbol{r}}\|^2}.
\end{aligned}
$$

From Eqs. 2.20, the derivatives of the position vector can be written in the following form for a constant heading angle:

$$
\dot{\boldsymbol{r}} = \begin{bmatrix} v \cdot cos\gamma cos\psi_0 \\ v \cdot cos\gamma sin\psi_0 \\ v \cdot sin\gamma \end{bmatrix}, \tag{5.5}
$$

$$
\ddot{\boldsymbol{r}} = \begin{bmatrix} \dot{v} \cdot cos\gamma cos\psi_0 - v \cdot \dot{\gamma} sin\gamma cos\psi_0 \\ \dot{v} \cdot cos\gamma sin\psi_0 - v \cdot \dot{\gamma} sin\gamma sin\psi_0 \\ \dot{v} \cdot sin\gamma + v \cdot \dot{\gamma} cos\gamma \end{bmatrix} = \begin{bmatrix} (c_1 cos\gamma - c_2 cos\phi_0 sin\gamma) cos\psi_0 \\ (c_1 cos\gamma - c_2 cos\phi_0 sin\gamma) sin\psi_0 \\ c_1 sin\gamma + c_2 cos\phi_0 cos\gamma - g_0 \end{bmatrix}. \tag{5.6}
$$

Using the first integrals in Eqs. 2.21, these derivatives can be written in terms of γ (flight-path angle) which allows us to get the invariants as the functions of the flight-path angle.

5.2 Special Cases

In this section, some special cases of aircraft's motion will be studies. The assumptions made above are considered to be invalid for this section. The roll, pitch, and yaw angles are denoted by ϕ, θ, and ψ respectively.

5.2.1 Rotational Motion

Roll maneuver: $\dot{\phi} \neq 0,\ \dot{\theta} = 0,\ \dot{\psi} = 0$

Consider the motion that the aircraft performs a roll maneuver. In this case, the first and the second invariants can be written in terms of bank and sideslip angles. The other four invariants would be zero:

$$\begin{aligned} i_1 &= \|\boldsymbol{\omega}\| = \dot{\phi}, \\ i_2 &= \|\dot{\boldsymbol{r}}\| = v = \eta_4(a + b\ sin\ \lambda)^{-1} exp\left[\frac{2A}{d_1} arctan \frac{a\ tan\ \bar{\lambda} + b}{d_1}\right], \\ i_3 &= i_4 = i_5 = i_6 = 0. \end{aligned} \tag{5.7}$$

Pitch maneuver: $\dot{\phi} = 0,\ \dot{\theta} \neq 0,\ \dot{\psi} = 0$

In this case, the aircraft performs a pitch maneuver, and the invariants will take the following form:

$$\begin{aligned} i_1 &= \dot{\theta}\|cos\ \phi_0 - sin\ \phi_0\|, \\ i_2 &= \dot{y}, \\ i_3 &= i_4 = i_5 = i_6 = 0, \end{aligned} \tag{5.8}$$

where ϕ_0 is a constant bank angle.

Yaw maneuver: $\dot{\phi} = 0,\ \dot{\theta} = 0,\ \dot{\psi} \neq 0$

For this case of aircraft's motion, the rotational and the translational velocity vectors can be written as [54]

$$\boldsymbol{\omega} = [0\ 0\ (cos\theta_0 cos\phi_0 + cos\theta_0 sin\phi_0 - sin\theta_0)]^{\mathrm{T}}, \quad \boldsymbol{v} = [\dot{x}\ \dot{y}\ \dot{z}]^{\mathrm{T}}, \tag{5.9}$$

where θ_0 is a constant pitch angle.
The invariants will be as follows

$$\begin{aligned} i_1 &= \dot{\psi}\|cos\theta_0 cos\phi_0 + cos\theta_0 sin\phi_0 - sin\theta_0\|, \\ i_2 &= \dot{z}, \\ i_3 &= i_4 = i_5 = i_6 = 0. \end{aligned} \tag{5.10}$$

5.2.2 Translational Motion

When the aircraft has only the translational velocity, the screw axis would be in the direction of this velocity vector, and the only nonzero invariant would be the invariant 2. Depending on the choice of the $\boldsymbol{e_x}$ unit vector, it could be either positive or negative:

$$\begin{aligned} i_1 &= 0, \\ i_2 &= v = \eta_4(a + b\ sin\ \lambda)^{-1} exp\left[\frac{2A}{d_1} arctan\frac{a\ tan\ \bar{\lambda} + b}{d_1}\right], \\ i_3 &= i_4 = i_5 = i_6 = 0. \end{aligned} \tag{5.11}$$

5.3 Simulation

5.3.1 Simulation Setup

Since the change in weight is considered negligible, c_1 and c_2 constants in Eq. (2.19) represent the accelerations along the wind axis and the lift axis respectively. In most cases, the lift acceleration is greater than the gravitational acceleration which means that $(c_2 cos\phi_0)^2 > g_0^2$. Without loss of generality, the following values for the constants can be chosen to simulate the obtained results [45]:

$$\begin{aligned} &m = 40kg, \quad g_0 = 9.81m/sec^2, \quad S = 21.55, \quad K = 0.073, \quad Cd_0 = 0.0223, \\ &Ar = 5.1, \quad \alpha_{0L} = 0.1, \quad \alpha_T = 0.1, \quad c_1 = 1, \quad c_2 = 10, \quad \psi_0 = \pi/4, \quad \phi_0 = 0. \end{aligned}$$

5.3.2 Graphical Relationship Between Parameters

Due to the high nonlinearity in the equations for both invariants and flight-path angle, it is hard to get an explicit relationship between these parameters. Thus, the author tried to establish an implicit relationship through the graphs obtained in MATLAB. The profiles of the ISM invariants with respect to flight-path angle and angle of attack are shown in Figure 5.1.
Figure 5.2 shows the diagrams for the angle of attack, velocity magnitude, and thrust.
The invariants were tested by changing the constant value of the bank angle. From the simulation

results, the profiles of the invariants in Figure 5.3 show that the increase in the bank angle decreases the rate of the invariants except for i_2 and i_6 (we cannot see a significant change in invariant 6). The invariants have also been tested by changing the heading angle, and it turned out to be that the invariants don't depend on the heading angle if it is constant, i.e., the motion is on a vertical plane.

5.3.3 Discussions of Simulation Results

Figure 5.1 represents the invariants with respect to the angle of attack and flight path angle considering the bank and heading angles constant. It can be seen that the first invariant (i_1) is proportional to the angle of attack, and increases parabolically as the flight-path angle increases. The second invariant is zero for any values of γ and α under the assumptions considered. The third invariant fluctuates in a small interval (nearly zero), and the interval becomes wider as γ increases. The 4th invariant fluctuates in the interval [-1000,1000], and the interval shrinks as γ increases. The fifth invariant changes between 0 and 1.5, and it is hard to evaluate the change of interval. The invariant 6 changes dramatically with random fluctuations, and tends to infinity when $\boldsymbol{\omega}$ goes to zero. To provide a smooth transition through the special points where $\boldsymbol{\omega}$ or its time derivative goes to zero, the author is currently working on several methods. One of the methods that are being considered is to set a critical interval for $\boldsymbol{\omega}$ (angular velocity) and start changing the direction of the $\boldsymbol{e_x}$ unit vector towards the translational velocity when $\boldsymbol{\omega}$ enters the critical interval. Finalizing this study on these methods and applying them to the current system is one of the future works. The relationship between Thrust, velocity magnitude, angle of attack, and flight path angles is shown in Figure 5.2. In Figure 5.3, how the change in the bank angle affects the invariants and other parameters is described. It can be seen that the increase in the bank angle decreases the rate of invariants with respect to the flight path angle. In the result, the fluctuation ranges in the diagrams of invariants 3-6 have decreased significantly.

5.4 Applications of the Study

The proposed approach to the control and guidance problems in UAVs can increase the efficiency of autonomous UAVs and have potentially important contributions to the field of aerodynamics. The results of the study can also be utilized in flight dynamics in addressing agricultural and environmental problems where UAVs are used to collect imagery data and to monitor the fields of interest. One example is the work done by the NASA-funded EPSCoR Project at the Kauai Coffee field in 2018 where the plantation was monitored and high-resolution imagery data was collected along with other applications [55]. These kinds of applications can help farmers increase productivity and enhance agriculture. By integrating the obtained results to the GNC algorithm in autonomous UAVs, they can be used to perform specific tasks such as searching in and monitoring

flood zones in residential areas of Oahu and the other Hawaiian Islands. Moreover, the improved GNC allows us to use the UAVs not only for monitoring the vegetation and coffee plantations in the islands and developing the map of them but also for collecting other different types of data by approaching the target more closely.

The relationships between the invariants and dynamic and control parameters obtained in this study can be used to improve the performance of a dynamical system. For example, the explicit and implicit relationships between the parameters allow us to evaluate the degrees of importance of their impact in performing various maneuvers. It is expected that a control and guidance system utilizing the ISM concept and the ISA may allow us to extend the areas of UAV applications to a wide range of environmental and other societal problems where the autonomy of the UAV plays a significant role.

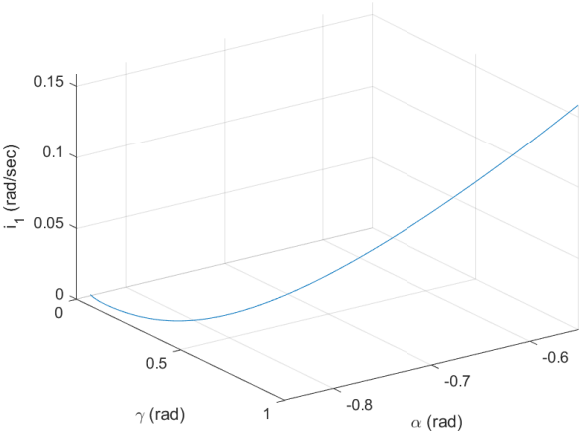

(a) i_1

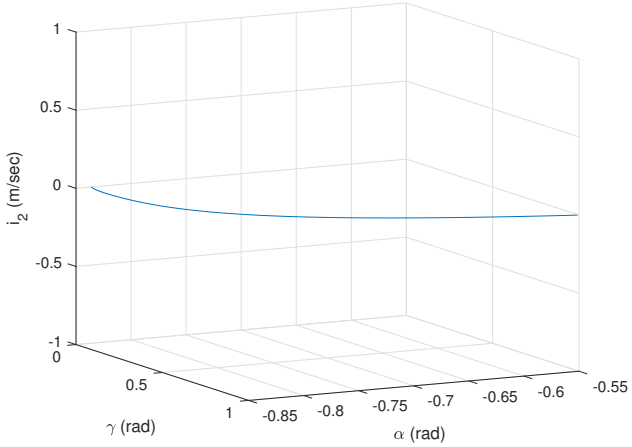

(b) i_2

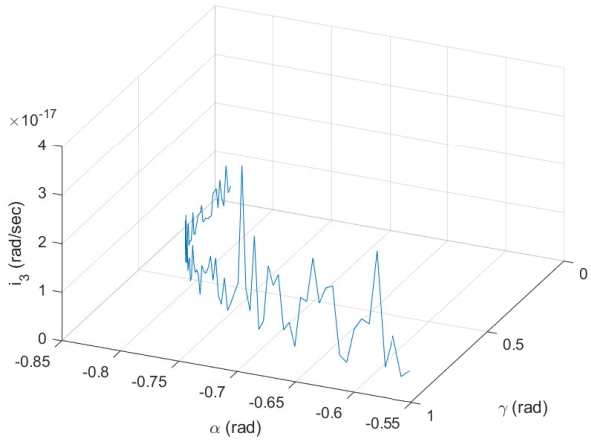

(c) i_3

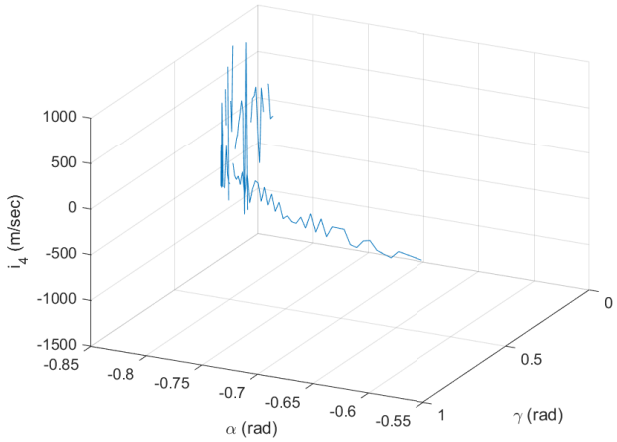

(d) i_4

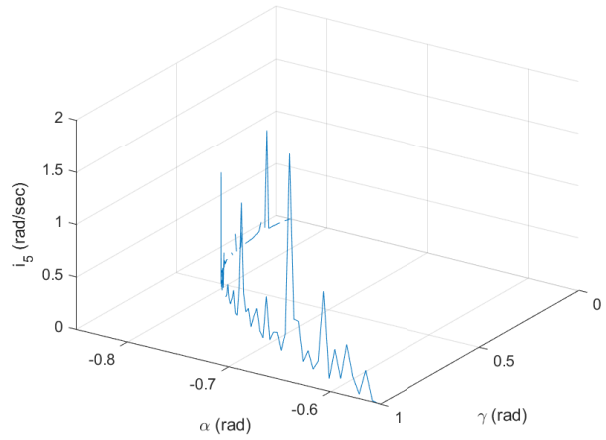

(e) i_5

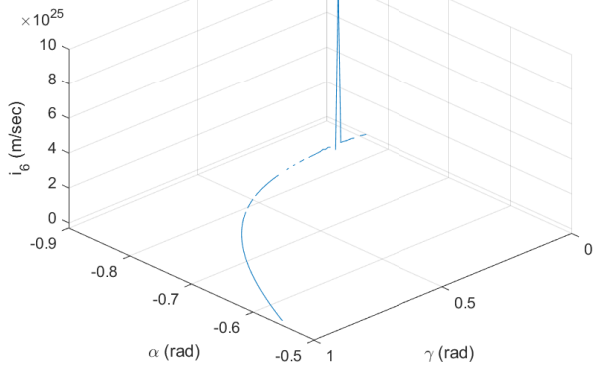

(f) i_6

Figure 5.1: Invariants vs Angle of attack and Flight path angle

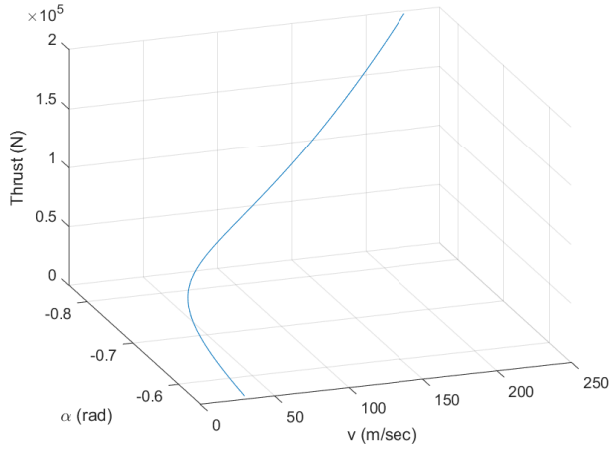

(a) Thrust vs Angle of attack vs Velocity magnitude

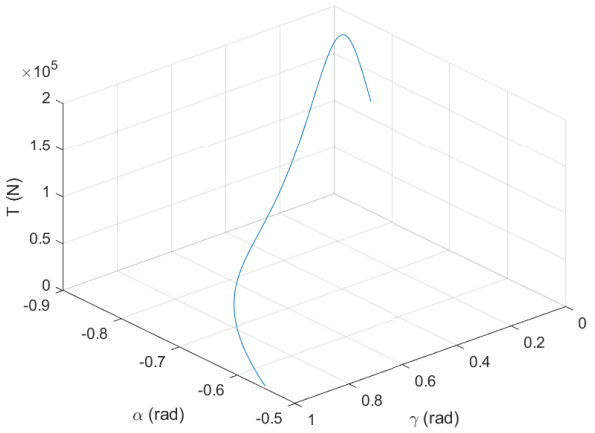

(b) Thrust vs Angle of attack vs Flight path angle

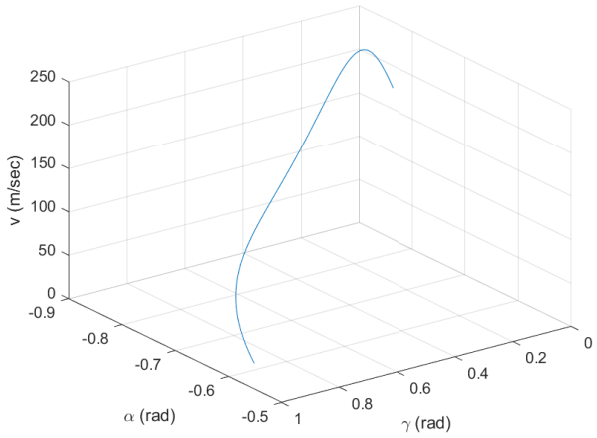

(c) Velocity vs Angle of attack vs Flight path angle

Figure 5.2: Control parameters and velocity

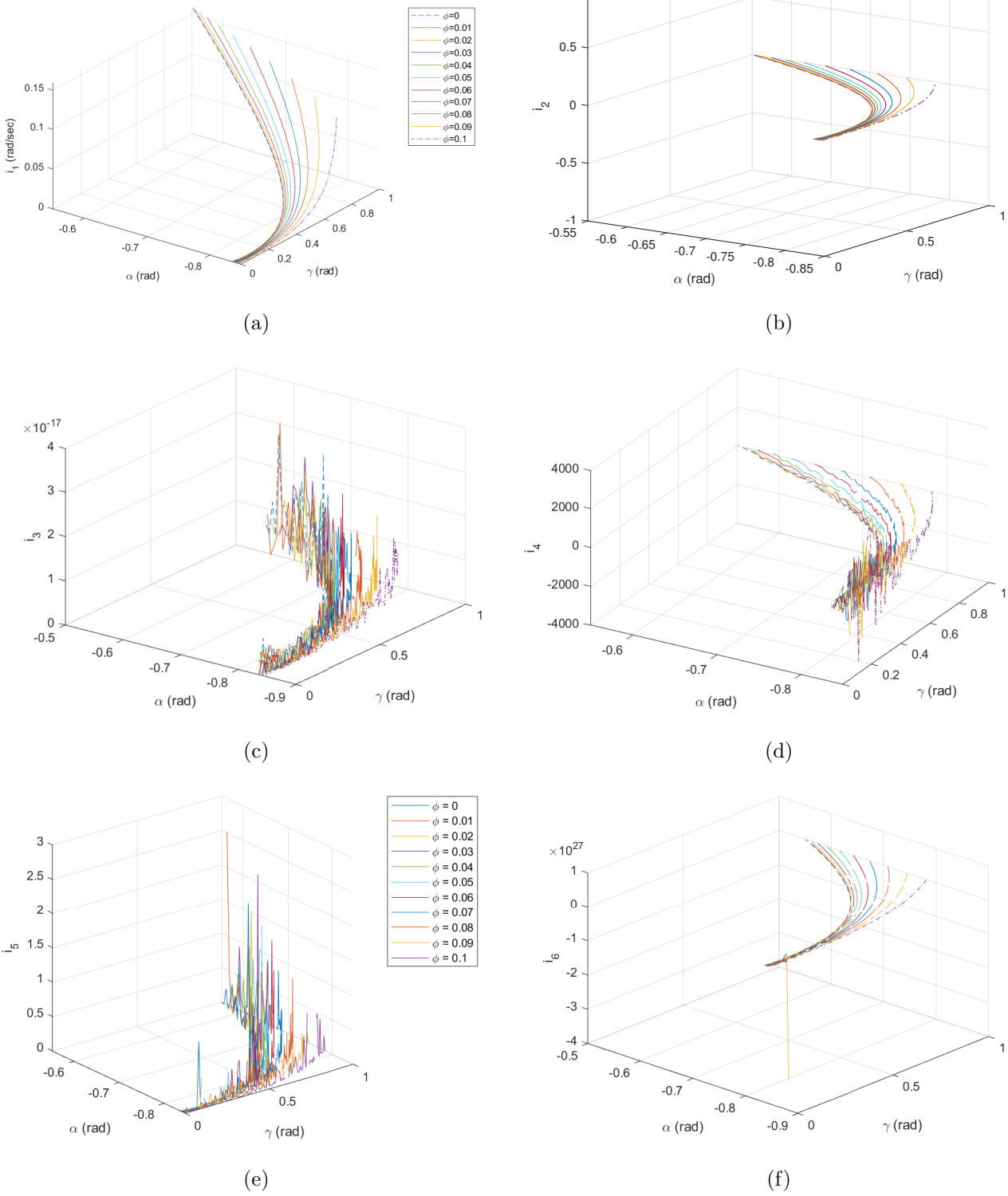

Figure 5.3: Invariants vs bank angle

CHAPTER 6
GUIDANCE VIA ISM INVARIANTS

The guidance methods have been developed by employing the general explicit guidance, quartic polynomial, Lyapunov's second method, the vision-based guidance, and other numerical, approximate, and analytical methods [5], [23]-[36]. The original and general concept of explicit guidance was first obtained by George Cherry, an MIT staff member, and called E-guidance [56]. The E-guidance is defined by the following equation

$$\boldsymbol{a_{com}} = \boldsymbol{c_1}(\boldsymbol{\xi_c}, \boldsymbol{v_c}, \boldsymbol{\xi_d}, \boldsymbol{v_d}, t_c, t_d)p_1(t) + \boldsymbol{c_2}(\boldsymbol{\xi_c}, \boldsymbol{v_c}, \boldsymbol{\xi_d}, \boldsymbol{v_d}, t_c, t_d)p_2(t) - \boldsymbol{g}, \tag{6.1}$$

where $\boldsymbol{a_{com}}$ - commanded translational acceleration, $\boldsymbol{\xi_c},\ \boldsymbol{v_c},\ \boldsymbol{\xi_d},\ \boldsymbol{v_d}$ - position and velocity vectors respectively (subscripts c and d indicate *current* and *desired*), $\boldsymbol{g}$ is gravitational acceleration, $p_1(t)$ and $p_2(t)$ are arbitrary functions of time, c_1 and c_2 are dynamic coefficients [56], [26].
By adjusting this equation, Alan Klumpp, an Apollo engineer, obtained his quartic polynomial lunar descend guidance formula, which was used for all Apollo missions [26]. One of the long-term goals of this research is to modify the guidance concepts given by Cherry and Klumpp by utilizing the ISM invariants. In the proposed method, the guidance commands will be computed using the invariants' current and desired states, and the expressions can be written in the following form:

$$\begin{aligned}
\boldsymbol{a_{com}} &= \boldsymbol{c_1}(\boldsymbol{\xi_c}, \boldsymbol{v_c}, \boldsymbol{\xi_d}, \boldsymbol{v_d}, t_c, t_d)p_1(i_k^c, i_k^d) + \boldsymbol{c_2}(\boldsymbol{\xi_c}, \boldsymbol{v_c}, \boldsymbol{\xi_d}, \boldsymbol{v_d}, t_c, t_d)p_2(i_k^c, i_k^d) - \boldsymbol{g}, \\
\boldsymbol{\epsilon_{com}} &= \boldsymbol{c_3}(\boldsymbol{\xi_c}, \boldsymbol{v_c}, \boldsymbol{\xi_d}, \boldsymbol{v_d}, t_c, t_d)p_3(i_k^c, i_k^d) + \boldsymbol{c_4}(\boldsymbol{\xi_c}, \boldsymbol{v_c}, \boldsymbol{\xi_d}, \boldsymbol{v_d}, t_c, t_d)p_4(i_k^c, i_k^d) - \boldsymbol{\omega} \times \boldsymbol{I\omega} - \boldsymbol{G_g},
\end{aligned} \tag{6.2}$$

where $\boldsymbol{\epsilon}$ is rotational acceleration command, i_k - ISM invariants, $k = 1 - 6$, t_c, t_d - current and desired moment of time, $\boldsymbol{\omega}$ - rotational velocity vector, $\boldsymbol{I}$ - inertia matrix, $\boldsymbol{G_g}$ is gravity gradient vector [26]. For small and medium UAVs where the flight altitude ranges up to around 5000 m, this gradient vector can be considered negligible since the change in the gravitational acceleration is very small (look at Figure 6.1). $p_{1-4}(i^c, i^d)$ are arbitrary functions, and they can be chosen based on the dynamical model. The analysis of these functions is one of the future works.
The current (i^c) and desired (i^d) states of the invariants can be found from the current and desired velocity vectors and their derivatives

$$\begin{aligned}
i_k^c &= f_k(\boldsymbol{v_c}, \dot{\boldsymbol{v}}_{\boldsymbol{c}}, \ddot{\boldsymbol{v}}_{\boldsymbol{c}}, \boldsymbol{\omega_c}, \dot{\boldsymbol{\omega}}_{\boldsymbol{c}}, \ddot{\boldsymbol{\omega}}_{\boldsymbol{c}}), \\
i_k^d &= f_k(\boldsymbol{v_d}, \dot{\boldsymbol{v}}_{\boldsymbol{d}}, \ddot{\boldsymbol{v}}_{\boldsymbol{d}}, \boldsymbol{\omega_d}, \dot{\boldsymbol{\omega}}_{\boldsymbol{d}}, \ddot{\boldsymbol{\omega}}_{\boldsymbol{d}}),
\end{aligned} \tag{6.3}$$

where $\boldsymbol{v}$ and $\boldsymbol{\omega}$ are linear and angular velocity vectors (subscripts c and d indicate *current* and *desired*).
The proposed GNC algorithm with ISM invariants is described in Figure 6.2.

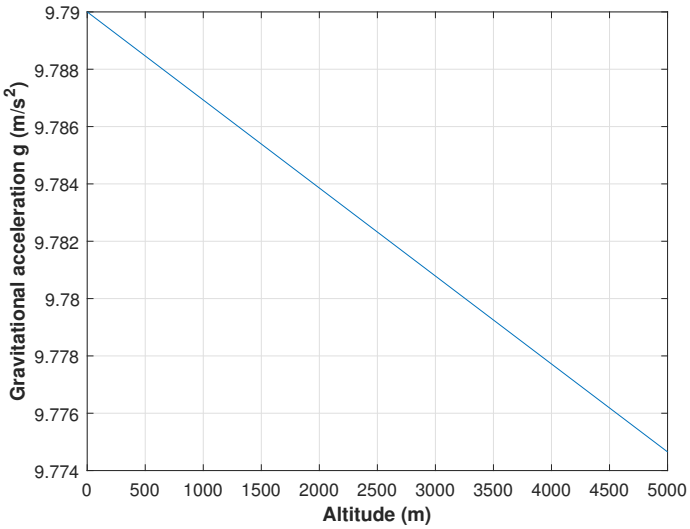

Figure 6.1: Gravitational acceleration vs Altitude

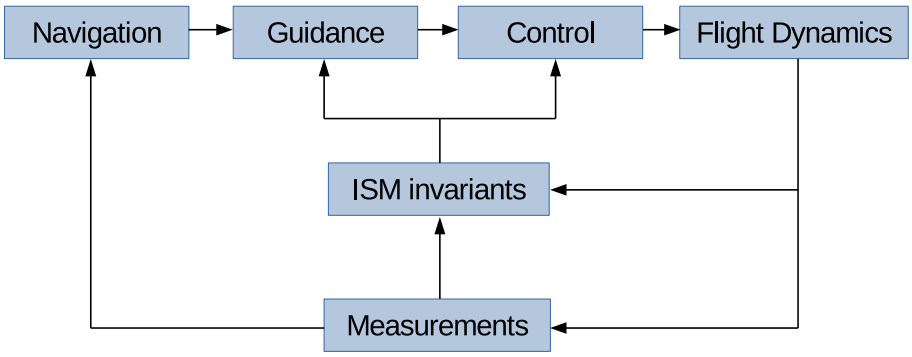

Figure 6.2: Proposed GNC algorithm with ISM invariants

CHAPTER 7
CONCLUSIONS

7.1 Conclusions of the Study

The expressions for the ISM invariants have been derived for the quadcopter and fixed-wing UAV motion. The invariants have been determined in terms of control parameters. An implicit relationship between the invariants and the flight dynamic parameters was established. The graphical representations of the implicit relationship were obtained and analyzed. The transfer methodology from the invariants to the traditional parameters has been developed.

The results show that the invariants are very sensitive to even small changes in motion, which can be useful in decreasing the error in control, guidance, and navigation problems. In addition, the invariants are independent of the heading angle which means that for any constant heading angle the invariants are found to be the same. It is also shown that the increase in the bank angle decreases the rate of the invariants with respect to the flight-path angle.

The obtained results can be used to evaluate the parameters in control and guidance problems, develop invariant-based control and guidance systems.

7.2 Future works

So far, the ISM invariants have been analyzed along with the kinematic and dynamic parameters, UAV dynamic model, and control parameters. The future work includes the application of the expressions obtained for the invariants in terms of dynamic parameters to guidance equations. Second, the utilization of the invariant-based expressions for the control and guidance equations in navigation problems can be useful to reduce systematic error. Third, analyze the invariants in the optimal control problem, and see if they are useful to improve the performance index.

APPENDIX A
EXPRESSION FOR V_3

$$
\begin{aligned}
v_3 =& \frac{[\dot{\boldsymbol{\omega}} \times \boldsymbol{h_2} + \boldsymbol{\omega} \times \boldsymbol{h_3}] \cdot [\|\boldsymbol{\omega}\|^2 \cdot (\boldsymbol{h_4} + \boldsymbol{\omega} \times \dot{\boldsymbol{v}}) - 2(\boldsymbol{\omega} \cdot \dot{\boldsymbol{\omega}}) \cdot \boldsymbol{h_1}]}{\|\boldsymbol{\omega}\|^3 \cdot \|\boldsymbol{h_2}\|^2} \\
&+ \frac{\boldsymbol{\omega} \times \boldsymbol{h_2} \cdot [\|\boldsymbol{\omega}\|^2 \cdot (\ddot{\boldsymbol{\omega}} \times \boldsymbol{v} + 2(\dot{\boldsymbol{\omega}} \times \dot{\boldsymbol{v}}) + \boldsymbol{\omega} \times \ddot{\boldsymbol{v}}) - 2(\|\boldsymbol{\omega}\|^2 + \boldsymbol{\omega} \cdot \ddot{\boldsymbol{\omega}})\boldsymbol{h_1}]}{\|\boldsymbol{\omega}\|^3 \cdot \|\boldsymbol{h_2}\|^2} \\
&- \left[\frac{3(\boldsymbol{\omega} \cdot \dot{\boldsymbol{\omega}})}{\|\boldsymbol{\omega}\|} + \frac{2\|\boldsymbol{\omega}\|\boldsymbol{h_2} \cdot \boldsymbol{h_3}}{\|\boldsymbol{h_2}\|^2}\right] \\
&\times \frac{\boldsymbol{\omega} \times \boldsymbol{h_2} \cdot [\|\boldsymbol{\omega}\|^2 \cdot (\boldsymbol{h_4} - \boldsymbol{\omega} \times \dot{\boldsymbol{v}}) - 2(\boldsymbol{\omega} \cdot \dot{\boldsymbol{\omega}})\boldsymbol{h_1}]}{\|\boldsymbol{\omega}\|^4 \|\boldsymbol{h_2}\|^2} + \frac{\boldsymbol{h_4} \cdot \boldsymbol{\omega}}{\|\boldsymbol{\omega}\|^3}
\end{aligned} \tag{A.1}
$$

where

$$\boldsymbol{h_1} = \boldsymbol{\omega} \times \boldsymbol{v}, \boldsymbol{h_2} = \boldsymbol{\omega} \times \dot{\boldsymbol{\omega}}, \boldsymbol{h_3} = \boldsymbol{\omega} \times \ddot{\boldsymbol{\omega}}, \boldsymbol{h_4} = \dot{\boldsymbol{\omega}} \times \boldsymbol{v}.$$

APPENDIX B
EXPRESSIONS FOR I_4 AND I_6

$$
\begin{aligned}
i_4 =& [\ (\|\boldsymbol{L}\|^2(P_z\tau_y/I_y - P_y\tau_z/I_z + L_yF_z/I_y - L_zF_y/I_z) - 2q_1(L_yP_z/I_y - P_yL_z/I_z)) \\
&\times (L_y\tau_z - L_z\tau_y)/I_yI_z \\
&+ (\|\boldsymbol{L}\|^2(P_x\tau_z/I_z - P_z\tau_x/I_x + L_zF_x/I_z - L_xF_z/I_x) - 2q_1(L_zP_x/I_z - P_zL_x/I_x)) \\
&\times (L_z\tau_x - L_x\tau_z)/I_xI_z \\
&+ (\|\boldsymbol{L}\|^2(P_y\tau_x/I_x - P_x\tau_y/I_y + L_xF_y/I_x - L_yF_x/I_y) - 2q_1(L_xP_y/I_x - P_xL_y/I_x)) \\
&\times (L_x\tau_y - L_y\tau_x)/I_xI_y] \\
&\quad /mq_2\|\boldsymbol{L}\|^4
\end{aligned}
\tag{B.1}
$$

$$
\begin{aligned}
i_6 =& [\ L_x(P_z\tau_y/I_xI_y - P_y\tau_z/I_xI_z) + L_y(P_x\tau_z/I_yI_z - P_z\tau_x/I_yI_x) \\
&+ L_z(P_y\tau_x/I_xI_z - P_x\tau_y/I_yI_z)\ ]/m\|\boldsymbol{L}\|^2 \\
&- \frac{d}{dt}[\ \{(\|\boldsymbol{L}\|^2(P_z\tau_y/I_y - P_y\tau_z/I_z + L_yF_z/I_y - L_zF_y/I_z) - 2q_1(L_yP_z/I_y - P_yL_z/I_z)) \\
&\times (L_y(L_x\tau_y - L_y\tau_x)/I_xI_y^2 - L_z(L_z\tau_x - L_x\tau_z)/I_xI_z^2) \\
&+ (\|\boldsymbol{L}\|^2(P_x\tau_z/I_z - P_z\tau_x/I_x + L_zF_x/I_z - L_xF_z/I_x) - 2q_1(L_zP_x/I_z - P_zL_x/I_x)) \\
&\times (L_z(L_y\tau_z - L_z\tau_y)/I_yI_z^2 - L_x(L_x\tau_y - L_y\tau_x)/I_yI_x^2) \\
&+ (\|\boldsymbol{L}\|^2(P_y\tau_x/I_x - P_x\tau_y/I_y + L_xF_y/I_x - L_yF_x/I_y) - 2q_1(L_xP_y/I_x - P_xL_y/I_x)) \\
&\times (L_x(L_z\tau_x - L_x\tau_z)/I_zI_x^2 - L_y(L_y\tau_z - L_z\tau_y)/I_zI_y^2)\} \\
&/mq_2^2\|\boldsymbol{L}\|^3\ ]
\end{aligned}
\tag{B.2}
$$

where

$$
\begin{aligned}
q_1 &= L_x\tau_x/I_x^2 + L_y\tau_y/I_y^2 + L_z\tau_z/I_z^2, \\
q_2 &= \sqrt{(L_y\tau_z - L_z\tau_y)^2/(I_yI_z)^2 + (L_z\tau_x - L_x\tau_z)^2/(I_xI_z)^2 + (L_x\tau_y - L_y\tau_x)^2/(I_xI_y)^2},
\end{aligned}
$$

$L_{x,y,z}, P_{x,y,z}, \tau_{x,y,z}, F_{x,y,z}$ - components of vectors $\boldsymbol{L}, \boldsymbol{P}, \boldsymbol{\tau}$ and $\boldsymbol{F}$ respectively.

APPENDIX C
PUBLICATIONS AND SEMINARS

C.1 Journal papers

Ref	Journal	Status
[53]	Aerospace Science and Technology	Under Review
N/A	Journal of Dynamic Systems, Measurement, and Control	Ready for Submission

Table C.1: List of Journal Papers

C.2 Seminars

[ME 691 Seminar] **Unmanned Aerial Systems Guidance and Control Utilizing Instantaneous Screw Motion Invariants**, 11/03/2021.

BIBLIOGRAPHY

[1] Thomas J. Mueller and James D Delaurier. Aerodynamics of small vehicles. *Annual Review of Fluid Mechanics*, 35:89–111, 2003.

[2] J.D. Schutter. Invariant description of rigid body motion trajectories. *Journal of Mechanisms and Robotics*, 2010.

[3] G. Mozzi. *Discorso Matematico sopra il Rotamento Momentaneo dei Corpi.* Stamperia del Donato Campo, Napoli, 1763.

[4] M. Ceccarelli. Screw axis defined by giulio mozzi in 1763. *Ninth World Congress IFToMM*, pages 3187–3190, 1995.

[5] D. Azimov. Synthesis of optimal precision guidance system for controllable dynamical systems using instantaneous screw motion invariants. 2013. Private Communications.

[6] T. Luukkonen. Modelling and control of quadcopter. 2011.

[7] A. Gibiansky. Quadcopter dynamics, simulation, and control. 2012.

[8] Syed Ali Raza and Wail Gueaieb. Intelligent flight control of an autonomous quadrotor. In *Motion Control*, pages 245–264. IN-TECH, 2010.

[9] S.L. Waslander C.J. Tomlin G.M. Hoffman, H. Haung. Quadrotor helicopter flight dynamics and control: Theory and experiment. Technical report, American Institute of Aeronautics and Astronautics, 2007.

[10] F. M. Dimentberg. *The screw calculus and its applications in mechanics.* Moskva Nauka.

[11] J. Angeles. Automatic computation of the screw parameters of rigid-body motions. part i: Finitely-separated positions. *Journal of Dynamic Systems, Measurement, and Control*, pages 32–38, 1986.

[12] J. Angeles. Automatic computation of the screw parameters of rigid-body motions. part ii: Infinitesimally-separated positions. *Journal of Dynamic Systems, Measurement, and Control*, pages 39–43, 1986.

[13] United States Airforce. Autonomous horizons. Technical report, Department of the Air Force, 2015.

[14] Christopher Eaton, Edwin Chong, and Anthony Maciejewski. Multiple-scenario unmanned aerial system control: A systems engineering approach and review of existing control methods. *Aerospace*, 3:1, 01 2016.

[15] Xiang Yu and Youmin Zhang. Sense and avoid technologies with applications to unmanned aircraft systems: Review and prospects. *Progress in Aerospace Sciences*, 74:152–166, 01 2015.

[16] Hanseob Lee, Seokwoo Jung, and David Shim. Vision-based uav landing on the moving vehicle. In *2016 International Conference on Unmanned Aircraft Systems (ICUAS)*, pages 1–7, 06 2016.

[17] D. Ghose M. Suresh. Group coordination and path replan tactics in gps denied environments. In *2016 International Conference on Unmanned Aircraft Systems (ICUAS)*, pages 31–39, 2016.

[18] Georg Rudnick and Axel Schulte. Scalable autonomy concept for reconnaissance uavs on the basis of an htn agent architecture. In *2016 International Conference on Unmanned Aircraft Systems (ICUAS)*, pages 40–46, 2016.

[19] Cameron T. Rogers, Charles Noren, and John Valasek. Heterogeneous multi-vehicle modular control framework with payload integration. In *2017 International Conference on Unmanned Aircraft Systems (ICUAS)*, pages 264–270, 2017.

[20] Amer Al-Radaideh and Liang Sun. Self-localization of a tethered quadcopter using inertial sensors in a gps-denied environment. In *2017 International Conference on Unmanned Aircraft Systems (ICUAS)*, pages 271–277, 2017.

[21] Sarah Ismail and Liang Sun. Decentralized hungarian-based approach for fast and scalable task allocation. In *2017 International Conference on Unmanned Aircraft Systems (ICUAS)*, pages 23–28, 2017.

[22] Abhishek Manjunath, Parwinder Mehrok, Rajnikant Sharma, and Ashwini Ratnoo. Application of virtual target based guidance laws to path following of a quadrotor uav. In *2016 International Conference on Unmanned Aircraft Systems (ICUAS)*, pages 252–260, 2016.

[23] Brett E. Barkley and Derek A. Paley. Cooperative bayesian target detection on a real road network using aerial vehicles. In *2016 International Conference on Unmanned Aircraft Systems (ICUAS)*, pages 53–61, 2016.

[24] Parikshit Maini and P. B. Sujit. Path planning for a uav with kinematic constraints in the presence of polygonal obstacles. In *2016 International Conference on Unmanned Aircraft Systems (ICUAS)*, pages 62–67, 2016.

[25] Marius Beul and Sven Behnke. Analytical time-optimal trajectory generation and control for multirotors. In *2016 International Conference on Unmanned Aircraft Systems (ICUAS)*, pages 87–96, 2016.

[26] D. Azimov. Autonomous guidance for space vehicles using instantaneous screw motion invariants. 2016. Private Communications.

[27] Vaibhav Darbari, Saksham Gupta, and Om Prakash Verma. Dynamic motion planning for aerial surveillance on a fixed-wing uav. In *2017 International Conference on Unmanned Aircraft Systems (ICUAS)*, pages 488–497, 2017.

[28] Mark Garber, Sivakumar Rathinam, and Rajnikant Sharma. A grid-based path planning approach for a team of two vehicles with localization constraints. In *2017 International Conference on Unmanned Aircraft Systems (ICUAS)*, pages 516–523, 2017.

[29] Tom Stian Andersen and Raymond Kristiansen. Quaternion guidance and control of quadrotor. In *2017 International Conference on Unmanned Aircraft Systems (ICUAS)*, pages 1567–1601, 2017.

[30] Evan Kawamura. *Integrated Targeting, Guidance, Navigation, and Control for Unmanned Aerial Vehicles*. PhD thesis, University of Hawaii at Manoa, Honolulu, HI, 2020.

[31] Dilmurat Azimov and John Allen. Analytical model and control solutions for unmanned aerial vehicle maneuvers in a vertical plane. *Journal of Intelligent & Robotic Systems*, 91:725–733, 2017.

[32] Seokwon Lee, Jihoon Lee, Somang Lee, Hyunjin Choi, Youdan Kim, Seungkeun Kim, and Jinyoung Suk. Sliding mode guidance and control for uav carrier landing. *IEEE Transactions on Aerospace and Electronic Systems*, 55(2):951–966, 2019.

[33] Sebastian Benders, Andreas Wenz, and Tor Arne Johansen. Adaptive path planning for unmanned aircraft using in-flight wind velocity estimation. In *2018 International Conference on Unmanned Aircraft Systems (ICUAS)*, pages 483–492, 2018.

[34] Egidio D'Amato, Immacolata Notaro, Luciano Blasi, and Massimiliano Mattei. Smooth path planning for fixed-wing aircraft in 3d environment using a layered essential visibility graph. In *2019 International Conference on Unmanned Aircraft Systems (ICUAS)*, pages 9–18, 2019.

[35] Reza Radmanesh, Manish Kumar, Donald A. French, and David W. Casbeer. Towards a pde-based large-scale decentralized solution for path planning of uavs in shared airspace. *Aerospace Science and Technology*, 105:105965, 2020.

[36] Ya Liu, Fan Zhang, Panfeng Huang, and Xiaozhen Zhang. Analysis, planning and control for cooperative transportation of tethered multi-rotor uavs. *Aerospace Science and Technology*, 113:106673, 03 2021.

[37] Yiheng Liu, Honglun Wang, Jiaxuan Fan, Jianfa Wu, and Tiancai Wu. Control-oriented uav highly feasible trajectory planning: A deep learning method. *Aerospace Science and Technology*, 110:106435, 2021.

[38] Alexey A. Munishkin, Dejan Milutinović, and David W. Casbeer. Stochastic optimal control navigation with the avoidance of unsafe configurations. In *2016 International Conference on Unmanned Aircraft Systems (ICUAS)*, pages 211–218, 2016.

[39] Antonio Matus-Vargas, Gustavo Rodriguez-Gomez, Jose Martinez-Carranza, and Arturo Muñoz-Silva. Numerical optimization techniques for nonlinear quadrotor control. In *2017 International Conference on Unmanned Aircraft Systems (ICUAS)*, pages 1309–1315, 2017.

[40] Thomas S. Alderete. Simulator aero model implementation. 1997.

[41] Y.A. Çengel and J.M. Cimbala. *Fluid Mechanics: Fundamentals and Applications*. McGraw-Hill Education, 2018.

[42] Online scource. Airfriction. http://hyperphysics.phy-astr.gsu.edu/hbase/airfri.html.

[43] Hakim Bouadi and M. Tadjine. Nonlinear observer design and sliding mode control of four rotor helicopter. *Int Journal of Eng. and Applied Science*, 3, 01 2007.

[44] Laloui Derafa, Tarek Madani, and Abdelaziz Benallegue. Dynamic modelling and experimental identification of four rotors helicopter parameters. pages 1834 – 1839, 01 2007.

[45] Hull D.G. *Atmosphere, Aerodynamics, and Propulsion*, pages 43–78. Springer Verlag, Heidelberg, Germany, 2007.

[46] D. Azimov. Example of the integration of atmospheric flight equations. *Journal of Aircraft*, 48:1722–1732, 09 2011.

[47] Karl J Astrom and Tore Hagglund. *Advanced PID control*. ISA, Advanced PID control, 2006.

[48] Ismail Can Dikmen, Aydemir Arisoy, and Hakan Temeltas. Attitude control of a quadrotor. *2009 4th International Conference on Recent Advances in Space Technologies*, pages 722–727, 2009.

[49] A. Tayebi and S. McGilvray. Attitude stabilization of a four-rotor aerial robot. In *2004 43rd IEEE Conference on Decision and Control (CDC) (IEEE Cat. No.04CH37601)*, volume 2, pages 1216–1221 Vol.2, 2004.

[50] Hassan K Khalil. *Nonlinear systems; 3rd ed.* Prentice-Hall, Upper Saddle River, NJ, 2002.

[51] Jonas Persson and Lennart Soder. Comparison of three linearization methods. 01 2008.

[52] Efrain Ibarra and Pedro Castillo. Nonlinear super twisting algorithm for uav attitude stabilization. In *2017 International Conference on Unmanned Aircraft Systems (ICUAS)*, pages 640–645, 2017.

[53] J. Abdinabiev and D. Azimov. Quadcopter kinematics, dynamics and control solutions utilizing instantaneous screw motion invariants. *Aerospace Science and Technology*, 2021. (in rewiev).

[54] J. Strzalko, J. Grabski, Przemyslaw Perlikowski, Andrzej Stefanski, and Tomasz Kapitaniak. Dynamics of gambling: origins of randomness in mechanical systems. *Proceedings of the Institution of Mechanical Engineers, Part C: Journal of Mechanical Engineering Science*, 225:1756 – 1756, 2009.

[55] EPSCoR Project. Autonomous control technology for unmanned aerial systems with agricultural and environmental applications in central pacific islands. *University of Hawaii at Manoa*, 2018.

[56] George W. Cherry. A general, explicit, optimizing guidance law for rocket-propelled spaceflight. 1964.

[57] Z. Cao J. Zheng P. Wang, Z. Man and Y. Zhao. Dynamics modelling and linear control of quadcopter. *2016 International Conference on Advanced Mechatronic Systems (ICAMechS)*, pages 498–503, 2016.

[58] A. P. Markeev. *Theoretical mechanics (Teoreticheskaya mekhanika, (in Russian))*. Moskva Nauka.

[59] Satadal Ghosh, Duane T. Davis, Timothy H. Chung, and Oleg A. Yakimenko. Development and testing of the intercept primitives for planar uav engagement. In *2017 International Conference on Unmanned Aircraft Systems (ICUAS)*, pages 286–293, 2017.

[60] Zhixiang Liu, Laurent Ciarletta, Chi Yuan, Youmin Zhang, and Didier Theilliol. Path following control of unmanned quadrotor helicopter with obstacle avoidance capability. In *2017 International Conference on Unmanned Aircraft Systems (ICUAS)*, pages 304–309, 2017.

[61] Mohammad A. Alsharif, Yunus E. Arslantas, and Matthew S. Hölzel. Advanced pid attitude control of a quadcopter using asynchronous android flight data. In *2017 International Conference on Unmanned Aircraft Systems (ICUAS)*, pages 1602–1607, 2017.

[62] Francesco Cappello, Roberto Sabatini, and Subramanian Ramasamy. Aircraft dynamics model augmentation for rpas navigation and guidance. In *2016 International Conference on Unmanned Aircraft Systems (ICUAS)*, pages 457–464, 2016.

[63] Dilmurat Azimov and Evan Kawamura. Real-time guidance, navigation and control framework for fixed-wing aircraft maneuvers in a vertical plane. In *2018 International Conference on Unmanned Aircraft Systems (ICUAS)*, pages 621–630, 2018.

[64] S. K. K. Hari, S. Rathinam, S. Darbha, K. Kalyanam, S. G. Manyam, and D. Casbeer. Efficient computation of optimal uav routes for persistent monitoring of targets. In *2019 International Conference on Unmanned Aircraft Systems (ICUAS)*, pages 605–614, 2019.

[65] Charles Blouin, Eric Lanteigne, and Wail Gueaieb. Optimal control for the trajectory planning of micro airships. In *2017 International Conference on Unmanned Aircraft Systems (ICUAS)*, pages 885–892, 2017.

[66] C.R. de Cos, J.Á. Acosta, and A. Ollero. Relative-pose optimisation for robust and nonlinear control of unmanned aerial manipulators. In *2017 International Conference on Unmanned Aircraft Systems (ICUAS)*, pages 999–1005, 2017.

[67] Vladimir Dobrokhodov. *Kinematics and Dynamics of Fixed-Wing UAVs*, pages 243–277. Springer Netherlands, Dordrecht, 2015.

[68] M. Asselin. *Flight in the Vertical Plane*, pages 103–128. AIAA Education Series, Wright-Patterson AFB, Ohio, 1965.

[69] H. Antoulas A. Bishop R. Nonlinear approach to aircraft tracking problem. *AIAA J Guidance, Control and Dynamics*, 17:1124–1130, 1994.

[70] Hugh Harrison Hurt. Aerodynamics for naval aviators. 1965.

[71] Azimov D. M. Dubois-Matra O. Bishop, R. H. and C. Chomel. Analysis of planetary reentry vehicles with spiraling motion. In *International Conference, New Trends in Astrodynamics and Applications 3*, Princeton, NJ, 2006.

[72] Waqas Khan and Meyer Nahon. Dynamics modeling of a highly-maneuverable fixed-wing uav. 04 2013.

[73] Erlend M. Coates and Thor I. Fossen. Geometric reduced-attitude control of fixed-wing uavs. *Applied Sciences*, 11(7), 2021.

[74] Simon Watkins, Ravi S, and Loxton B. The effect of turbulence on the aerodynamics of low reynolds number wings. *Engineering Letters*, 18, 08 2010.